Korean J. Chem. Eng., 40(6), 1247-1267 (2023)
DOI: 10.1007/s11814-023-1440-0
pISSN: 0256-1115
eISSN: 1975-7220

REVIEW PAPER

Recent progress in the preparation, characterization, and applications of modified halloysite nanotubes as adsorbents for wastewater treatment

Zaharaddeen Nasiru Garba*,†, Abdurrashid Haruna, Abdulkadir Tanimu***, Binta Zakari Bello****, and Zakariyya Uba Zango*****,†**

*Department of Chemistry, Ahmadu Bello University, P.M.B. 1044, Zaria, Nigeria
**Department of Fundamental and Applied Sciences, Universiti Teknologi PETRONAS, 32610 Seri Iskandar, Perak Darul Ridzuan, Malaysia
***Centre for Refining and Advanced Chemicals, King Fahd University of Petroleum and Minerals, Dhahran 31261, Saudi Arabia
****Department of Chemical Engineering, Ahmadu Bello University Zaria, Nigeria
*****Institute of Semi-Arid Zone Studies, Al-Qalam University Katsina, P.M.B. 2137, Katsina, Nigeria
(*Received 18 August 2022 • Revised 10 November 2022 • Accepted 31 January 2023*)

Abstract–The application of halloysite nanotubes (HNTs) in water purification is attracting extensive attention because they are inexpensive raw materials with a hollow nanotubular structure in the sub-micrometer range, a large specific surface area, pore volume, pore size, and adequate hydroxyl groups on their surface, thus enhancing their ability to be modified. These modified halloysite nanotubes (m-HNTs) have been widely used for a variety of applications, including chemocatalysis, biocatalysis, antibacterial action, drug delivery, gas separation, and adsorbents for wastewater treatment. They were reported to have been produced using a variety of synthetic processes which include self-assembly/vacuum filtering, extraction, solution casting, dehydration condensation, thermal polycondensation, chemical vapor deposition, and hydrothermal carbonization. In this review, we focus on the compilation of the most recent developments in the manufacture of m-HNTs, their characterization and possible uses in wastewater treatment. Finally, we present our personal views on the opportunities and challenges of future researches involving m-HNTs, hoping to inspire more researchers into participating in this fascinating area.

Keywords: Halloysite Nanotubes, Preparation, Characterization, Adsorption, Wastewater Treatment

INTRODUCTION

The famous quote "a drop of water is worth more than a sack of gold to a thirsty man" well describes the significant value of fresh water rather than luxurious materials [1]. Due to increased industrialization and population growth around the world, water contamination directly affects the entire planet. Many dangerous chemicals, such as dyes, fertilizers, herbicides, medicines, nuclear wastes, and heavy metals, get into the water as a result of increasingly inevitable activities, which have a detrimental effect on both human health and the environment [2-4]. In addition, these contaminants present high level of toxicity even at low concentrations, constituting a major threat to fauna and flora [5].

Water pollution is a major concern of the United Nations agenda of 2030 toward achieving Sustainable Development Goals number 6 (SDGs), emphasizing clean water and sanitation [6]. The need for clean water, the most vital natural resource for everyday life, has increased as a result of water pollution. An effective and affordable treatment method is preferred from an energy and environmental standpoint to restore water quality. Major technologies of wastewater treatment exist since past decades and they include biological, physical, and chemical treatment methods [7-13]. However, these technologies suffer drawbacks which restrict their application in wastewater treatment. For instance, membrane separation and evaporation are pricey procedures, and industrial operations involving aerobic and anaerobic digestion demand high levels of skill. Additionally, some processes like coagulation and flocculation call for the use of significant amounts of chemicals, which could result in secondary by-products like sludge. The procedures, in theory, do not completely eliminate pollutants, and they require significant capital expenditure to clean wastewater. It is now vital to design an effective and long-lasting method for water purification due to the aforementioned negative consequences [14-16].

To realize this objective of developing an efficient wastewater treatment technique, the use of an adsorption technology for the removal of hazardous wastes via the application of nanotechnology has shown incredible potential in recent years. Adsorption technology, for example, is a technique of wastewater treatment that is currently gaining tremendous attention over the application of traditional materials employed for water decontamination [17,18]. Adsorption is regarded as an effective, affordable, sustainable, and straightforward process for removing waste materials from aqueous solutions. Adsorbent materials provide a number of benefits, including effective biodegradability in natural environments, a higher propensity

†To whom correspondence should be addressed.
E-mail: zngarba@abu.edu.ng, dinigetso2000@gmail.com

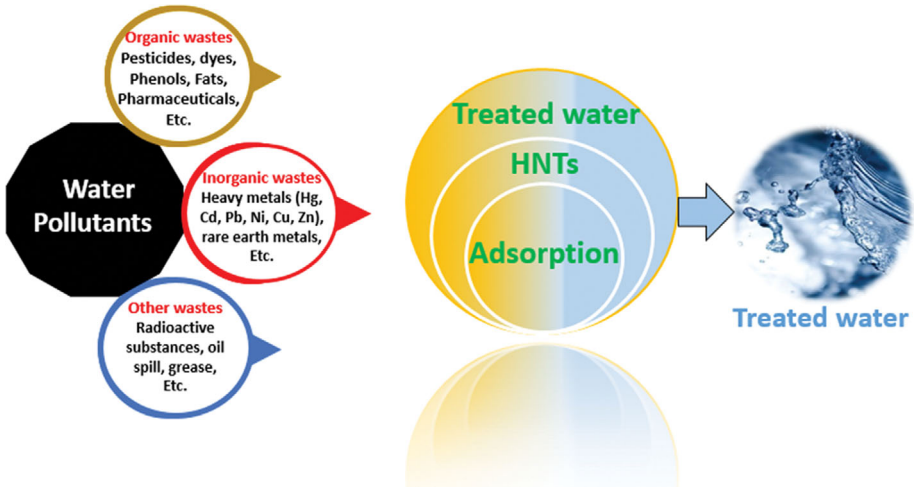

Fig. 1. Application of HNTs for the removal of various wastewater pollutants.

to adsorb waste materials, and ease of renewable resources [19]. In addition, adsorbents are readily available, eco-friendly, possesses high specific surface area, suitable pore volume and dimension, and can be easily prepared [20]. A breakthrough in the use of adsorption technology as an effective way to remove aqueous pollutants using inexpensive materials like agricultural wastes occurred in the last two decades, which is interesting and has produced amazing results [21]. For example, Allahkarami et al. [22] synthesized a magnetic lead-ferrite-activated carbon composite for the efficient removal of phenol from aqueous solutions. The adsorbent material demonstrated a high capacity, and after six cycles 85% of the adsorption capacity was maintained. A new technique of combining artificial neural networks (ANNs) with an optimization method is recently applied to predict the removal of pollutants [16]. The ANN model is performed on a trial-and-error basis and can be used with reasonable accuracy compared to classical models.

Furthermore, researchers used the adsorption process employing various adsorbents such as lignin [23], microcrystalline cellulose [15,24,25] zeolites [26], activated carbon [22,27-33], natural clay [34], chitosan [35], and many other chemically synthesized materials for wastewater purification [36,37]. As an important emerging technique, adsorption is highly effective in the extraction process and is easy to apply and recycle in a wide range of scientific fields [38].

Modified halloysite nanotubes (m-HNTs), as adsorbent materials for wastewater treatment, have recently been the focus of innovative research and advances because of their exceptional qualities, such as non-toxicity, porosity, and vast amounts readily available [39]. m-HNTs have shown extraordinary potential due to being environmentally benign and effective for wastewater treatment. Like carbon nanotubes (CNTs), which are commercially available nanomaterial with abundant surface OH groups and porous structure, HNTs are very similar to CNTs [40,41]. While CNTs are difficult to prepare and present high level of toxicity, HNTs are nontoxic, readily available, and their production in large quantity for industrial applications is rapidly increasing as water remediation technology [42-44]. HNT is a naturally available clay mineral that exists in the form of aluminosilicate ($Al_2Si_2O_5(OH)_4 \cdot nH_2O$) and is currently under extensive study due to its potential for remediation of wastewater. The application of HNTs for the removal of various wastewater pollutants is depicted in Fig. 1.

In terms of the electronic and chemical characteristics of HNTs, a structural difference exists between the inner and outer nanocrystal of the material [45]. For instance, the inner surface of HNT has a higher concentration of hydroxyl groups (Al-OH) and a positive charge, whereas the outer surface has a lower concentration of hydroxyl groups (Si-OH) and a negative charge. A few Si-OH groups (mainly Si-O-Si groups) are found on HNT nanomaterial, which is proof that the outer surface structure is more negatively charged due to the electronegativity of the oxygen atoms [46]. Following this, HNT demonstrates a better dispersibility to amalgamate a binary or ternary hybrids with other supporters, thereby lessening the concentration of -OH groups and charged surface. Noteworthy, review works have been widely published in this subject using various types of HNTs materials for wastewater remediation [45,47-49]. To enhance water quality by employing HNTs-based nanomaterials, it is tremendously recommended to discuss the structural modification and compositional characteristics of structure-activity relationship of m-HNTs. However, a focused review that describes the general properties of m-HNTs, their structure and types, preparation and modification techniques has yet to be reported. As such, this review aims to summarize and discuss the m-HNTs based on past and recent works, their characterization, and their current applications as adsorbent materials. A comparison of m-HNTs with other adsorbent materials that are used for wastewater treatment has also been provided. Ultimately, the challenges and future outlook have been put forward, while providing a new research direction for applying m-HNTs in wastewater treatment.

PREPARATION AND MODIFICATION OF HNTs NANOCOMPOSITES

Nanostructured materials have at least one of their dimensions in the range of 1-100 nm [50-53], and owing to the nano-sized of HNTs and good heat resistance, HNTs with natural nanoclay` structure have demonstrated fascinating properties for numerous

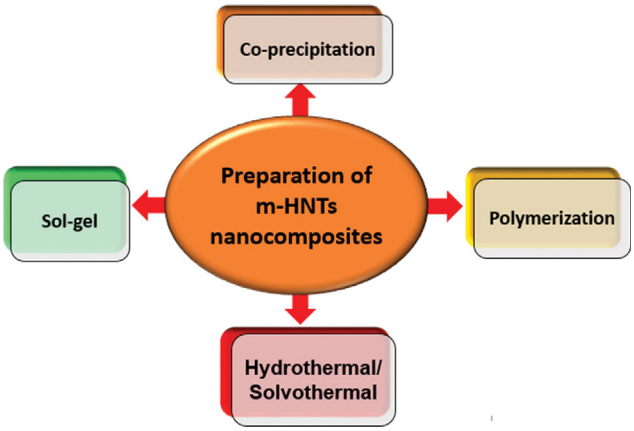

Fig. 2. Some preparation methods of m-HNTs nanocomposites [37].

technology applications [54]. Due to the low cost, non-toxicity, biocompatibility, and unique tubular hollow structures, HNT nanomaterials are efficient for the formation of composites with other compounds [55,56]. Saadat et al. carried out a recent study and indicated the potential of developing HNTs-based nanocomposites for wastewater treatment, wound healing, surface decontamination, and the treatment of microbial infections [57]. There are various methods of preparation of m-HNTs nanocomposites (Fig. 2).

A summary of the modification strategy, properties as well as the potential applications of HNTs are highlighted in Table 1.

There have been numerous studies of combined natural clay materials for wastewater treatment.

For instance, recent technological advancements have made it possible to design and create an effective adsorbent for the removal of phosphates [75]. The authors synthesized a functional HNTs with ZnO nanoparticles possessing dendrite-like structures for the adsorption of waste materials. The formation of the dendrite structures improved the grasp of phosphate molecules present in an aqueous solution. Zinc oxide nanoparticles were specifically coated onto the surface of HNTs resulting in the availability of more adsorption sites. Their findings suggested a new benchmark for the scavenging of phosphate molecules from wastewater due to the coating of HNT with ZnO nanoparticles, which consequently enhanced the adsorption affinity. The adsorption capacity of ZnO-HNTs exhibited an exceptionally high phosphate capacity of 97.3 mg $P \cdot g^{-1}$ under the equilibrium phosphate concentration of 346 mg $P \cdot L^{-1}$, which is most superior to other reported phosphate adsorbents. Masindi et al. reported the synthesis of HNTs-bentonite clay/magnesite material by ball milling and calcination method. The obtained material was explored for the adsorptive removal of chromium ions from real tannery wastewater. The authors reported that the incorporation of the support materials significantly improved the adsorption capacity of HNTs [76]. Even though different particle sizes were visible, the shape of the bentonite clay and the tubular rod-like architectures of the HNTs remained the same at two different magnifications of 100 and 200 nm.

Yadav et al. reported a similar result [77]. From the BET results obtained in the work that showed a specific area of 35.8 m^2/g, the value slightly increased to 37.9 m^2/g after adsorption of chromium ions from the wastewater. Interestingly, an increase in the surface area denotes the potential of the material for secondary use. Precipitation, ion exchange, and adsorption were demonstrated as the key parameters governing the mechanisms of chromium ion removal.

Türkeş and Sağ Açıkel [78] prepared magnetic HNT-chitosan nanocomposites employing the co-precipitation method. The produced nanoadsorbent was fully characterized and obtained the diameter and length of the material to be 116 and 774.92 nm, respectively. The adsorption of MB dye pollutant was achieved by using sustainable, environmentally friendly, and low-cost nanocomposites. It is well established that the adsorption kinetics and equilibrium of the dye are represented by the Freundlich and Redlich-Peterson models. Further, the material exhibited superior magnetic property with a magnetization value of 22.1 emu/g. Their work revealed that due to the nanostructured size of the magnetically synthesized material, its recovery from the wastewater using an external magnetic field has been demonstrated. In another development, Lee et al. carried out sol-gel preparation of photocatalyst-based HNTs doped with TiO_2 and La^{3+} ion. Herein, the HNT was employed as a support material for La-doped TiO_2 to improve the degradation of dye pollutants. The synergistic effect of combining these materials increased the adsorption efficiency of the substrates ~3 times higher than TiO_2 nanoparticles [79]. Indeed, the doping of TiO_2 with La^{3+} ions decreased the band gap of TiO_2 from 3.5 to 3.01 eV; the integration of HNTs further increased the visible light absorption of the material with a reduction of band gap to 1.5 times. In addition, the degradation process employing HNT decorated material enhanced the local dye concentration nearby the photocatalyst through the electrostatic interaction. This was reported to boost the photocatalytic activity by ~3 times higher. Remarkably, the catalyst showed efficient recyclability of five times without loss in activity. Numerous m-HNTs have been synthesized and applied for the efficient removal of waste materials from wastewater [80-83].

CHARACTERIZATIONS OF THE HNTs

Various researchers employed a wide range of complementary techniques, which include XRD, FTIR, Raman, XRF, EDX, ICP-OES, SEM, TEM, and N_2-adsorption-desorption isotherm in order to study and understand the structure and properties of the m-HNTs.

1. Chemical Structure (XRD, FTIR, Raman)

The greatest success of material science and engineering lies in its ability to identify and index the chemical structure of newly discovered or synthesized material in various indexing platforms. X-ray diffraction (XRD) has been very helpful in this regard. Subsequently, the indexed XRD diffraction pattern is used as a fingerprint of the new material. Therefore, XRD is a powerful technique for identification of materials based on their indexed XRD patterns. In addition, the material structure, crystallinity, crystal size and shape, crystal orientation and crystal defects have been obtained after careful analysis of the X-ray diffraction patterns [84]. Like other two-layered aluminosilicate clays, HNT is crystalline material and its X-ray diffraction pattern has since been indexed in the International Centre for Diffraction Data (ICDD) (JCPDS Card No. 29-1487) [85,86]. The XRD of HNT has two main diffraction

Table 1. Summary of the modification techniques, properties and potential applications of m-HNTs

Type of m-HNTs	Preparation method	Properties	Potential application	References
MXene/C-HNTs	Self-assembly/ Vacuum filtration	Enhanced permeability, stable channel after nano-intercalation, and enlarged interlayer channels	Pure water permeance, and dye desalination	[58]
Alginate-HNTs	Extraction	Sustainable, increased mechanical stability, and high adsorption capacity	Adsorbent for the removal of Pb(II) ions from wastewater	[59]
CCMHN	Stainless-steel vibratory ball milling	Particle sizes in the range of 20-50 nm, high adsorption capacity	Adsorption of MB from wastewater	[60]
Chitosan/HNTs-NH_2	Conventional solution casting method	Improved tensile strength and thermal stability	Industrial effluent degradation and biomedical applications	[61]
PLA/HNTs-TiO_2	Solution casting	Enhanced mechanical and tensile strengths, high efficiency of both Gram positive and Gram negative bacteria	Environmentally benign packaging materials	[62]
g-C_3N_4/TiO_2/HNTs	Sol-gel and calcination	High stability, outstanding photoelectric performance, rapid transfer and separation of e^-/h^+ pairs	Photocatalyst for the decomposition of ciprofloxacin	[63]
HNTs/BO	Dehydration condensation	High selectivity	Drug delivery for biomedical applications	[64]
GO-Gly/HNTs GO-GG/HNTs	Green solvent/ionic liquid	High adsorption capacity, and high recyclability	Adsorbent for the removal of Pb(II) ions from wastewater	[65]
CT-f-HNTs	Solution casting	Enhanced surface roughness, improved mechanical and thermal stability	Enzymatic decomposition and tissue engineering	[66]
TiO_2-Fe-HNTs	Hydrothermal treatment	High crystallinity, agglomeration of tubes, while the material increases the e^-/h^+ pair separation	Photo-adsorption of dyes, pharmaceutical wastes, and pesticides	[67]
HNTs/PE	Ball milling homogenization	High adsorption capacity, improved mechanical and thermal stability	Contributes to food safety, and acts as food packaging materials	[68]
Alginate/HNTs	Solution blending and cross-linking	Low cytotoxicity, increase in pore surface, high porosity, and surface area	Application in bone tissue engineering	[69]
g-C_3N_4/HNTs	Thermal polycondensation	High stability, increase in charge carrier formation, and reduced recombination rates of e^-/h^+ pairs	Photocatalytic removal of pollutants from wastewater	[70]
C+N-TiO_2/HNTs	Precipitation-dissolution-recrystallization	Formation of irregular morphology, reduced aggregation of particles, and formation of mesoporous structure	Photocatalytic degradation of MB dye pollutants	[71]
N-TiO_2/HNTs	Chemical vapor deposition	High crystallinity, high absorption, and photoactivity	Photocatalytic degradation of phenol from aqueous solution	[72]
HNTs-CeO_2-AgBr	Microwave-assisted	Crystalline, high stability and recyclability	Photocatalytic degradation of MO	[73]
HNTs/Fe_3O_4/carbon	Hydrothermal carbonization	High stability and good adsorption capability	MB adsorption from wastewater	[74]

patterns that are fingerprints of HNT structure, the first one usually appears in the range of 10-12° (2θ) and is ascribed to the d_{001} diffraction planes with a basal reflection of about 7 Å [87]. The second major diffraction pattern appears in the range of 24-26° (2θ) and corresponds to the d_{002} diffraction planes with a basal reflection of about 3.6 Å. Additional diffraction peaks that describe the tubular structure of HNT and presence of silica in the HNT material have also been reported. The tubular structure of HNT is characterized by intense d_{020} plane diffraction at 20° (2θ) with basal reflection of 4.5 Å [88], while the quartz silica shows weak d_{011} plane diffraction peak at 26.6° (2θ) [89]. Typically, the modification of HNT does not change its crystal structure or diffraction pattern to a reasonable extent. However, a slight shift in the peak position or decrease in peak intensity may be observed. For example, chemical

etching of HNT with H_2SO_4, CH_3COOH or CH_2=CHCOOH does not change its diffraction pattern [90-92], although when the acid treatment becomes aggressive, the crystal structure completely collapses [93]. It was also discovered that the acid treatment may lead to decrease in the intensity of d_{001} diffraction planes, and this has been linked to possible dealumination. Consequently, a corresponding increase in the intensity of d_{011} plane diffraction peak for quartz silica confirms that dealumination actually occurred [94,95].

Fourier transform infrared spectroscopy (FTIR) has also been useful in the elucidation of the chemical structure of materials. Because different chemical bonds in a molecule absorb different IR wavelengths, the kinds of chemical bonds in a material can be measured. Thus, FTIR is considered a powerful tool for identification and quantification of the functional groups (chemical bonds) in a material. Cheng et al. [96] described that the HNTs have two main peaks at 3,697 and 3,626 cm^{-1} that correspond to stretching vibrations of Al-OH in the lumen and the curled layer, respectively. The in-plane Si-O-Si is usually observed at approximately 1,040 cm^{-1}, whereas the Si-O and Al-O absorb mostly around 500 cm^{-1}. The presence of water stretching vibrations was used as a distinguishing factor between thermally treated and non-treated HNT. The stretching vibration band at 3,526 cm^{-1} was ascribed to water between the HNT layers, while the bands at 3,528 and 3,470 cm^{-1} correspond to the stretching vibration of water held in the interlayers. The band 1,637 cm^{-1} is attributed to bending vibrations of adsorbed water. Similarly, the grafting of poly(4-vinylpyridine) on HNTs was confirmed using FTIR spectroscopic analysis. The appearance of a strong absorption band at 3,451 cm^{-1} and moderate absorption band at 1,644 cm^{-1} for the NH_2 stretching vibration and in-plane bending vibration, respectively, in amine grafted HNTs indicated the presence of amino group. Further modification of amine functionalized HNTs to amide functionalized HNTs was confirmed by the appearance of broad band at 1,654-1,630 cm^{-1}, which was ascribed to tertiary amide. And the in-situ polymerization of amide functionalized HNTs with 4-vinylpyridine to form poly(4-vinylpyridine) functionalized HNTs is confirmed by the appearance of CH_2 stretching absorption band at 2,932 cm^{-1} and pyridine ring absorption band at 1,610 cm^{-1}.

Raman spectroscopy is another powerful technique to characterize the functional groups that are present in molecules [97,98]. More importantly, Raman spectroscopy has been very useful in the elucidation of atomic structure of solid samples. This is achievable due to the dependence of Raman scattering on the polarization and direction of the incident light and collected scattered light, in addition to the crystal symmetry and orientation of the solid samples. The micro-Raman spectroscopic method for determining local crystal orientation of silicon in metastable $Li_2Si_3O_7$ is a typical example of using Raman spectroscopy in the elucidation of atomic structure of solids [99]. Zsirka et al. [100] reported the Raman spectroscopic characterization of HNTs with the appearance of OH absorption bands at 3,705, 3,698, 3,630, 3,623, 3,617 cm^{-1} and 950, 938, 923, 915, 779, 728, 298, 238, 192 cm^{-1}. Absorption bands characteristics of Si-O were observed at 1,100, 844, 693, 540, 510, 396, 135 cm^{-1} and Al-O absorption bands were observed at 910, 442, 172, 156 cm^{-1} [101]. Similarly, the reaction progress in the functionalization of HNTs with polydopamine was monitored using surface-enhanced Raman spectroscopy (SERS) [102]. Fourier transform Raman spectra of clay minerals shows a broad band and a shoulder band at 143 and 127 cm^{-1}, respectively, that were assigned to the vibrational modes of O-Al-O and O-Si-O symmetric bends in HNTs [103].

2. Chemical Composition (Elemental Component Using XRF, EDX, ICP-OES)

The ability to determine the chemical composition of naturally occurring materials such as clays has led to the discovery of their significant roles in advancing materials science and technology research. The chemical compositions of materials have been measured using various techniques including X-ray fluorescence (XRF), energy dispersive X-Ray analysis (EDX) and inductively coupled plasma atomic emission spectroscopy (ICP-OES). Although highly sensitive, the ICP-OES is a destructive technique and the EDX system works when coupled to electron microscopy instrument. Therefore, XRF is mostly used for the determination of chemical composition of clay minerals such as HNTs. The XRF is a non-destructive technique that measures the fluorescent X-ray emitted from a sample when it is excited by a primary X-ray source. Since each element has a characteristic fluorescent X-rays that it produces, then the elements that are present in sample can be identified and quantified. As an aluminosilicate mineral with the structural formula $Al_2Si_2O_5(OH)_4 \cdot nH_2O$, the chemical composition of HNT is basically elemental percent of aluminum, oxygen, hydrogen and silicon. Yah et al. [104] reported that in a typical HNTs, the silicon atom is tetrahedrally bonded with oxygen atoms and the aluminum atom is coordinated with two hydroxyl groups and an additional oxygen atom. Garcia-Garcia et al. measured the chemical composition of HNTs using XRF and discovered that SiO_2 and Al_2O_3 constitute 53.57±0.64 and 44.57±0.67 percent respectively, totalling 98.3% of the total chemical composition of the HNTs [90]. The remaining percent is distributed among other oxides, such as P_2O_5, Fe_2O_3, SO_3, CaO, TiO_2 and MgO. Similar analysis by Ormanci-Acar et al. [105] showed that the SiO_2 and Al_2O_3 constitutes 44.00% and 37.59% of the HNTs, respectively. Based on these disparities in chemical compositions of HNTs, it follows that the clay source of the HNTs greatly determines its chemical composition. This is corroborated in a study where HNTs from six different sources (Camel Lake, Jarrahdale, Matauri Bay, Dragonite, Te Puke and Patch Clay) showed silica percent in the range 43.50-51.41 and alumina percent in the range 32.86-38.88 [106].

3. Morphology (SEM, TEM)

The morphological examination of HNTs, including particle size (length, inner/outer diameter, wall thickness), shape (particle and pore) and distribution, are carried out using electron microscopy analysis. The two most common electron microscopy techniques are scanning electron microscopy (SEM) and the transmission electron microscopy (TEM). While SEM cannot see features at the same level of detail as TEM, it is much faster, less restrictive, and can sometimes be performed with limited or no sample preparation. The TEM offers internal details of small samples at near-atomic resolution; thus is more informative and specific. As shown in Fig. 3, the HNTs have cylindrical, hollow and open-ended structure with average length of 500 nm and average diameter of 40-100 nm [105].

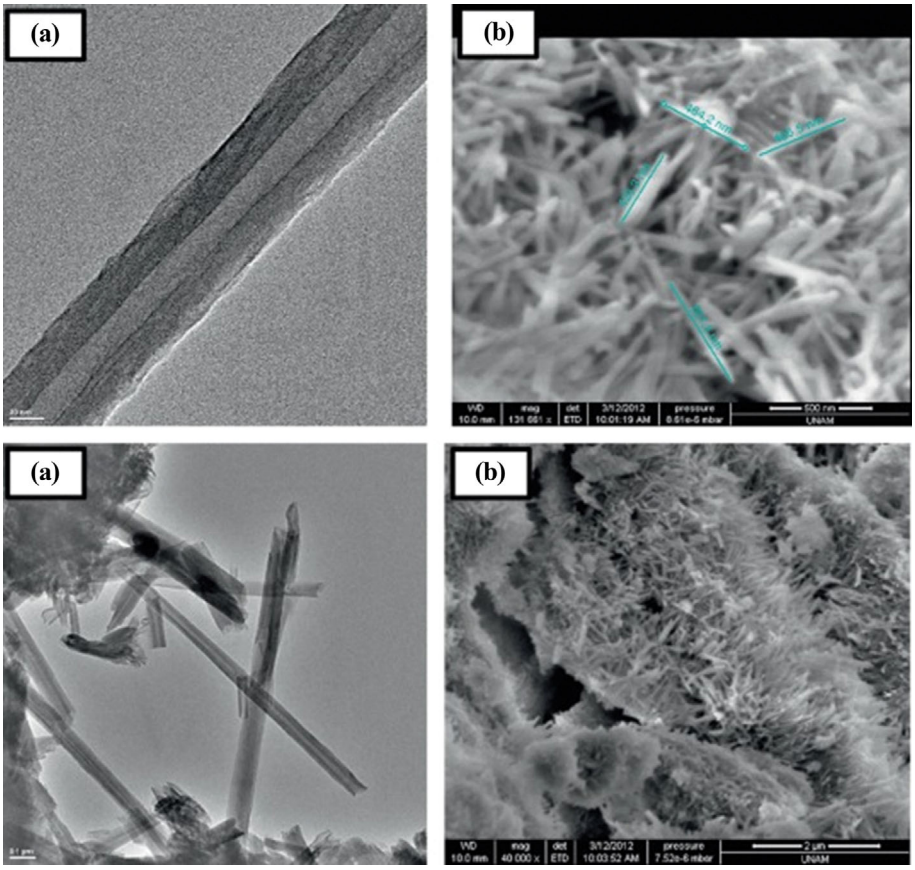

Fig. 3. Different magnification of (a) TEM and (b) SEM images of HNTs. Reproduced from ref. [105].

In another study, the high magnification TEM images of m-HNTs derived from different sources (Fig. 4) showed a predominantly tubular shape with outer diameter in the range of 20-200 nm, inner diameter 5-70 nm and length 50-5,000 nm [106]. As observed above, the tubular shapes were also cylindrical and open-ended, with an electron-transparent central lumen. Garcia-Garcia et al. [90] described the HNTs morphology as a tubed shape, with average lumen diameter of 13.8±1.4 nm and average external diameter of 50 nm, which is still within the range reported in the other studies.

4. Textural Properties (N_2-adsorption-desorption Isotherm)

The textural properties of materials are measured by their surface area and porosity, both of which are important factors that affect the adsorption properties of materials. These parameters are often determined using the adsorption-desorption isotherm approach, which depends on computing the monolayer coverage on the basis of the Brunauer-Emmett-Teller (BET) principle [107,108]. Although initially developed to describe multilayer adsorption of gas molecules on a solid surface [109], the BET principle has been effective in the measurement of surface area and porosity of solid materials. The measurement is done based on the adsorption isotherm of inert gases (mainly argon at 87 K or nitrogen at 77 K) over a relative pressure (defined as the ratio of gas equilibrium pressure to the gas saturation pressure) range of 0.05-1 [110]. The measured isotherms are converted to the linearized BET plot and the monolayer loading is determined accordingly. The pore volume and pore size distribution are typically calculated based on the Barrett-Joyner-Halenda (BJH) principle. While studying the effect of acid treatment on HNTs' surface area and porosity, it was discovered that the HNTs (both pristine and acid treated) showed type IV adsorption-desorption isotherm, which characterized them as mesoporous materials, and type H3 hysteresis loop, depicting their plate-like particles nature with slit-shaped pores [111]. In addition, the BET surface area of 52.9 m^2/g and pore volume of 0.146 cm^3/g was recorded for HNTs, which later increased to 132.4 m^2/g and a pore volume of 0.308 cm^3/g after sulfuric acid treatment. The surface area analysis of HNTs derived from nine different deposit sources showed that the surface area was within the range of 22.1-81.6 m^2/g, where Matauri Bay, Northland, New Zealand HNTs deposit source has the lowest surface area and Siberia, 85 km NW of Kalgoorlie, Western Australia HNTs deposit source has the highest surface area [112]. Similarly, Pasbakhsh et al. measured the BET surface area of six varieties of HNTs, which fall within the 22.1-81.6 m^2/g; however, their isotherms fit type II adsorption-desorption isotherm characterized by unrestricted monolayer-multilayer adsorption [106]. The HNTs pore size distribution was found to be broadly bimodal with two peaks: first peak at lower pore width and second peak at higher pore width. These peaks correspond to small and large pore sizes, the small pore size being attributed to internal/surface pores, including spaces between the overlaps of folded halloysite sheets and the large pore being attributed to the central lumen of the HNTs. On average, the HNTs have lumen space in the range of 10.7-39%, and because of the empty lumen structures,

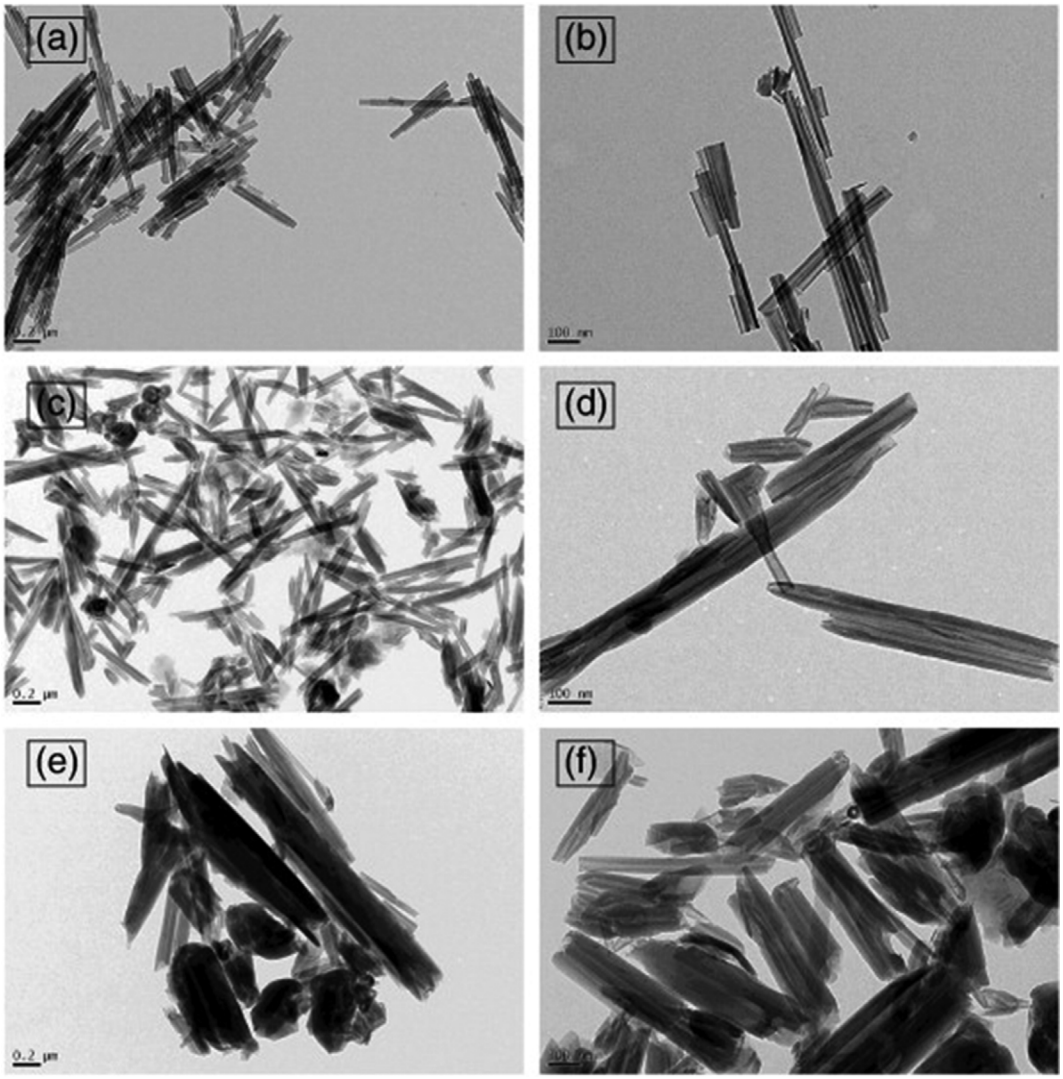

Fig. 4. TEM micrographs of halloysite samples; ((a) and (b)) Camel Lake; ((c) and (d)) Jarrahdale; ((e) and (f)) Matauri Bay. Reproduced from ref. [106].

the density of HNTs is relatively low (2.14-2.59 g/cm^3) [113,114]. The relatively low density of HNTs makes them convenient when preparing lightweight functionalized or composite materials for adsorption application.

APPLICATIONS OF m-HNTs AS ADSORBENTS

High porosity, structural stability, thermal and chemical resistance, and good water dispersity are the key fundamental properties for the prospects of the materials in adsorption studies. HNT has a tubular morphology, like that of carbon nanotubes, with size of 500-1,000 nm and inner diameter of 10-100 nm. The crystalline layer of the tube consists of aluminosilicate arranged in two-dimensional structures of tetrahedral and octahedral sheets. The tetrahedral sheet has siloxane [SiO_2] corner which is stacked with aluminate [AlO_6] edge of octahedral sheet and the internal [Al-OH] group. A monolayer of water [H_2O] also exists between the adjacent the siloxane and aluminate layers [115]. This rolled tubular arrangement offers HNTs a relatively high surface area and pore volumes ranging from. Also, the outer surface of HNTs possesses relatively lower Si-OH groups, hence it is negatively charged. While the inner layer of the lumen is positively charged due to the abundance of Al-OH groups. Thus, the variation of the surface charges to adsorb selectively, cationic, and anionic molecules onto their surface and lumen.

Thanks to the good crystalline layers and unique tubular structure of the HNTs, they could be subjected to various activation strategies, such as acid and alkaline activation, high temperature activation etc. Usually, the activation processes bring about dilation of the HNT pores and enhancement of its surface area and pore sizes for effective entrapment of guest molecules. For instance, the surface area of HNT reported by Zhang and co-workers was 40 m^2/g [116]. However, upon acid activation, the surface area was increased to 250 m^2/g. Thus, they concluded that direct treatment of the HNT with sulfuric acid led to the formation of wormlike nanopores by selectively etching the Al-OH tube wall of the HNT. Heat treat-

ment prior to acid etching has been reported as a good alternative technique to enhance the porosity of the HNT. Thus, the physicochemical and adsorptive property of Algerian HNT via heat treatment and acid leaching was reported by Belkassa et al. [93]. The heat and acid treatment strongly influences the mechanical strength of the HNT. Importantly the porosity of the HNT is greatly improved with the samples having the BET specific surface area of 60 and 503 m^2/g and total pore volume of 0.27 and 0.75 m^3/g for the native and treated HNT, respectively. Thus, the latter demonstrated effective adsorption performance for the removal of crystal violet [93]. Wang and co-workers described the alkali activation of HNT as efficient treatment to its adsorption property [117]. Thus the material exhibited higher porosity and good adsorption capacity for the removal of Al^{3+} and OFL from the aqueous medium.

The hydrophilic characteristic of HNTs with strongly negative charged surface and positively charged lumen brought about by the hydroxyl functional group (-OH) and Al^{3+}, respectively, allows for the compatibility of the materials to undergo derivatization and chemical reactions. The flexibility of the HNTs to undergo surface modifications with other functional groups, polymers surfactants etc., has inspired researchers to prepare composites and biopolymers of the HNTs for adsorptions applications. Usually, such functionalization results in the increase in number of actives pores and charged particles on the surface of the HNTs. For instance, the functionalization of HNTs with metal oxide nanoparticles materials to form nanocomposites results in the enhancement of the HNT specific surface area by introducing nanopores into the tubular HNT surface which aids its adsorption performance [118]. Supramolecular gel composite is fabricated by incorporating Fe_2O_3 into the nanotubular HNT pores which undergo surface reinforcement with 3-amino-n-propyltriethoxysilane. The resulting nanocomposite exhibits higher BET surface area pore size and pore volumes, magnetic property, good compressive strength for dye adsorption [119]. Incorporation of silver nanoparticles into tetraethylenepentamine (TEPA) functionalized HNT was reported by Kadir et al. [120]. The BET surface area was 30.1 and 86.4 m^2/g, while the corresponding pore volumes were 0.12 and 0.24 for the pristine HNT and the Ag/HNT/TEPA composite, respectively. The significant improvement in the porosity of the composite resulted in the effective adsorption and degradation of organic contaminants from water [120]. Synthesis of controllable polydopamine HNT composite for uranium (IV) adsorption was recently reported by Ou et al. [81]. The adsorption capacity of the HNT@PDA was greatly improved in comparison with the native HNT due to the improvement in the BET surface area, 28.92 and 40.15 m^2/g for the HNT and the composite, respectively [81]. Surfactant modified magnetic HNT using mixed hemimicelle was reported synthesized by Liu et al. for the solid-phase extraction and adsorptive determination of azo dyes from environmental water samples [121]. The adsorbent offers not only selective adsorption of the pollutants, but ease of regeneration due to its magnetic property.

Due to their low-cost, mechanical strength, tubular nanostructure, abstentious functionality, remarkable biocompatibility, HNT is widely explored to prepare membrane by combination with polymeric substances. Membrane technology has emerged as convenient method for entrapment of pollutants from environmental water. It helps to convert the shortcomings of leaching demonstrated by various powdered adsorbents. It offers good selectivity to various adsorbates in addition to its fouling effect. Also, it withstands harsh chemical environments, and has ease of application and regeneration for reusability. HNT membranes have shown superior adsorption capabilities for both organic and inorganic molecules, as reported by various researchers. The fabrication of HNT-polystyrene nanocomposite membrane by casting technique has been reported by Buruga et al. [122]. Varying the ratio of the HNT in the nanocomposite has improved the mechanical property and BET surface area of the membrane and resulted in the increase in its adsorption efficiency for the selective adsorption of pollutants and purification of real wastewater sample collected from pulp and paper mills [122]. HNT decorated polyvinylidene fluoride (PVDF) membrane was reportedly synthesized by Chen et al. using nature-inspired polyphenol chemistry via deposition of tannic acid (TA), polyethyleneimine (PEI) [123]. The synthesized TA/PEI/HNTs membrane has shown improved hydrophilicity and good antifouling performance for the removal of dyes and heavy metals for several number of adsorption cycles [123].

The potential of the HNTs and their composites for adsorption has been reviewed in various literatures. Early work reviewing the properties and application of HNTs was presented by Yuan and co-workers [112]. Even though the review discussed the occurrence, structural morphology, and surface modification of the HNTs, little was mentioned about their adsorption efficiency for wastewater remediation. Anastopoulos et al. [47] discussed the prosperous adsorption application of HNTs for pollutants and wastewater remediation. However, the work was limited to dyes and heavy metals adsorption, and the mechanism for the adsorption was not considered. Kausar et al. [124] also reviewed the general adsorption of clays for dyes remediation. Despite having described the optimization for the adsorption parameter, kinetics and thermodynamics, their findings focused more on bentonite, and little was mentioned about the kaolinite; thus, the limitation of their findings is clear for the HNTs and m-HNTs. In another development, the adsorption property of polymeric mixed-matrix membrane HNT for wastewater remediation was also reviewed [48]. The review discussed various fabrication methods for HNT membranes preparation with polymers such as polysulfone, polyether sulfone, polystyrene and polyvinylidene for the adsorption of pollutants from environmental waters. The remarkable features of the membranes, such as retention property, antibacterial property, permeability, fouling resistance, and mechanical strength, were elaborated. However, only a limited number of pollutants such as oils were referenced [48].

1. m-HNTs for Dyes Adsorption

Water pollution due to dyes has been a known environmental issue for decades. The wastewater from textiles, plastics, leather, petroleum, petrochemicals, and allied industries contains a broad spectrum of dyes with different chemical structures. Basically, all dyes are harmful to aquatic organisms and can pose a serious threat to humans when consumed or inhaled. Despite various attempts to remediate these toxic pollutants from the point of discharge and in the environmental waters, they remain detected due to their recalcitrant nature. Thus, adsorption as an efficient means

Table 2. Compilation of various m-HNTs as adsorbents for the removal of dyes

Adsorbent	Pollutant	Adsorption parameters				Highlights	References
		pH	Temp (K)	Adsorbate conc (mg/L)	Contact time		
HNT	MG	6-10	293-333	20-100	10-120 min	Higher adsorption capacity was achieved with the process best described as endothermic.	[132]
HNT	CV	-	293-328	10-80	0-240 min	The acid and heat treatment increased the surface area of the HNT for higher adsorption capacity.	[93]
HNT CuO-HNT	MR	1-9	-	9-21	0-100 min	CuO-HNT exhibited higher adsorption efficiency; thus it has shown higher methyl red uptake.	[118]
Hal-x-HCl Hal-x-NaOH	MB	2-12	298	100-550	24 hours	Adsorption was significantly affected by higher pH of the solution and the isotherms obeyed Redlich-Peterson model.	[115]
RGO/HNT	MB CR	2-10	293-313	30-100	0-12 hours	The adsorption efficiency increased with increasing the HNT ratio.	[49]
Ag_3PO_4-HNT	MB	-	-	1-5	0-60 min	The adsorption reached equilibrium within 30 minutes and obeyed Langmuir model.	[133]
HNTs-SO_3H/PES	RB 5	-	-	1,000	-	Higher adsorption capacity was achieved by the membrane associated to the sulfonic group	[134]
KH550/Fe_3O_4/HNTs	CR MO	-	-	-	48 hours	The adsorption mechanism can be ascribed to an interaction between the dye molecules and the -OH groups of the adsorbent.	[119]
MHNTs@C_{16}mimBr	MR MO	7	298	200	0-60 min	Langmuir model best described the process with higher adsorption capacity.	[121]
TA/PEI/HNTs	DY 4 DR 28 DB 14	3-11	-	50-800	10-270 min	The membrane maintained up to 90% adsorption efficiency even after 3 consecutive cycles.	[123]
HNT	MB	2-12	293-343	30-70	0-180 min	Rapid adsorption efficiency was achieved within short time.	[126]
HNT	CV	6	297-298	30-1,000	0-120 min	Heat treatment improved the diffusion of the dye to the active pores of the HNT.	[128]
HNT	MV	3-11	308-318	50-200	0-370 min	The process was described by rapid adsorption rate which increased with concentration of the dye.	[135]
HNT-Fe_3O_4	MB NR MO	-	-	28-37	0-24 hours	Magnetic separation was achieved easily without need for filtration.	[127]
CS-HNT	MB MG	-	-	40-240	0-120 min	The chitosan-HNT composite demonstrated higher adsorption efficiency than the individual adsorbent.	[129]
HNT	NR	2-7	298-318	50-400	0-240	The adsorption was strongly dependent on the HNT dosage, pH, and the contact time.	[136]

Table 2. Continued

Adsorbent	Pollutant	Adsorption parameters				Highlights	References
		pH	Temp (K)	Adsorbate conc (mg/L)	Contact time		
HNTs-SA and HNTs-SA-PAMAM	AR 1 MB	3-11	298-318	10-100	0-30	The functionalized HNT had higher adsorption capacity, which increased with temperature, pH and contact time.	[130]
Ag_2CO_3-HNT	MB	-	-	2-10	0-20	The adsorption was best described by pseudo-second order and proceeded via monolayer formation.	[137]
PEI/MHNTs	MB RhB	1-5	301	5-160	0-300	The membrane effectively removed the dyes proceeded by Langmuir formation.	[131]
PRGO/HNTs-PSS	RB 5	-	-	5-30	-	The membrane demonstrated higher adsorption of the dye at higher concentration.	[138]
HNT/PEI	MB	-	-	5	0-120	The surface coating of the HNT contributed to the efficient removal of the dye.	[139]
A-HNTs/GO	MO MB CV CR	-	-	20	0-5 days	The membrane demonstrated higher adsorption efficiency for all the dyes.	[140]
D-A-HNT	DR 28 DY 4 DB 14	-	-	50-800	30-180 min	Hydrophilic groups exist on the surface of the HNT and dopamine The contributed to the higher adsorption efficiency.	[141]
CCMHNT	MB	2-12	283-323	1-30	15-90 min	The adsorption occurs via electrostatic interaction between the cationic dye and the negative charge on the surface of the adsorbent.	[60]
A-HNT@PVDF	DR 28	3-11	-	100	30-180	The A-HNT@PVDF membrane effectively removed the dye than the pure PVDF.	[142]
HNTs/Fe_3O_4/Poly (DA+KH550)	MB	3-11	298-318	70-130	0-170	The HNTs skeleton, Fe_3O_4 and inner shell of the poly (DA+KH550) contributed to the high adsorption capacity of the dye.	[143]
HNT HNT/Kaolin HNT-CNF	CAS	3-11	-	50	0-24 hours	Combination of HNT with cellulose nanofibrils (CNF) significantly improved the adsorption of the dye.	[144]

of their removal has been proposed [125]. The prospect of the method has been highlighted in various literatures, partly due to its low-cost, ease of operation and seemingly countless number of adsorbents from both natural and synthetic sources.

The recorded success for the use of clay minerals in pollutant adsorption has been highlighted from the economic point of view and their potential to remove both organic and inorganic species from environmental waters as highlighted in Table 2. HNTs has been at the front line towards dye adsorption. Of the earliest work was the report of Zhao et al. [126] for MB adsorption using HNTs. Rapid adsorption was achieved within 30 min with an adsorption efficiency of 84.32 mg/g. The process was found to be pH dependent due to the increase in electrostatic attraction between the negatively charged surface of the adsorbent and positively charged dye [126]. Xie et al. [127] reported on the magnetic HNT reinforced by Fe_2O_3. The adsorption capacity for the HNT- Fe_2O_3 nanocomposites towards dyes removal was 18.44, 13.62 and 0.65 mg/g for MB, NR, and MO, respectively. The lower value for MO adsorption was due to the negative charge on the surface of the HNT at neutral conditions. However, the regeneration of the adsorbent was easily achieved by magnetic separation, without the need for filtration or centrifugation [127]. The adsorption of CV onto heat

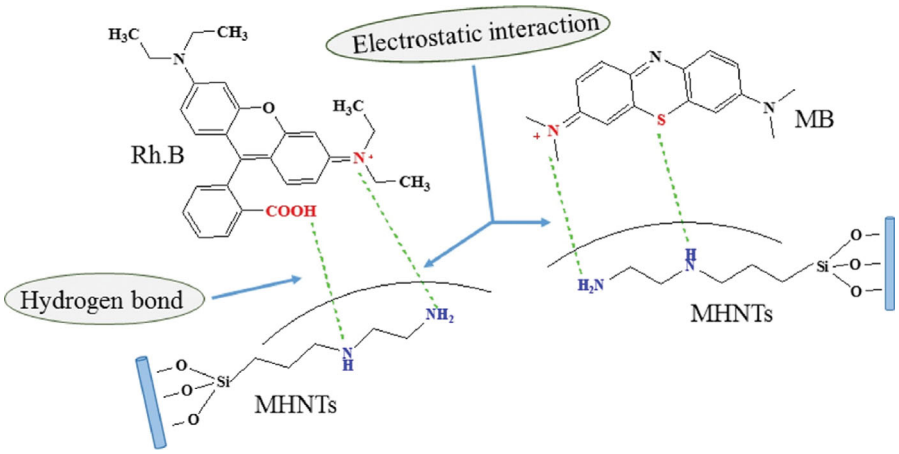

Fig. 5. Mechanism for RhB and MB adsorption onto HNT-AEAPTMS/PEI/PEG membrane (MHNTs). Reproduced from ref. [131].

treated HNT was reported by Krasilin et al. [128]. Complete adsorption took place within 120 mins with the adsorption kinetics governed by pseudo-second order model. The composite of HNT-CT hydrogel beads with higher stability was also synthesized by Peng et al. [129]. The addition of the HNT in the composite resulted in an increase in adsorption capacity for the removal of MB and MG. The adsorption was almost constant for five consecutive reusability, with the dyes composite achieving adsorption efficiency of over 95% [129]. Functionalization of HNT with poly(amidoamine) dendrimer (PAMMAM) and succinic acid anhydride (SA) significantly improved the performance of the HNT for both cationic and anionic dye adsorption. The HNT-SA-PAMMAM achieved relatively high removal rate for MB with adsorption efficiency of 99% [130]. An HNT membrane fabricated by diffusion induced phase inversion method with polyetherimide (PEI) and polyethylene glycol (PEG) was reported synthesized by Hebbar et al. [131]. Remarkable performance of the membrane towards MB and RhB dye removal was 97and 94%, respectively. The adsorption was described as pH dependent, in such a way that, at lower pH values (pH<Pzc), the membrane became more positively charged; thus, repulsion between the cationic dyes and the membrane surface occurred, which lowered the adsorption efficiency. However, increasing the pH of the solution (pH>Pzc) resulted in the higher adsorption of the dyes, attributed to deprotonation in the active sites of the membrane, which became negatively charged. Thus, electrostatic interaction between the cationic dyes and the negatively charged membrane surface was described as the predominant adsorption mechanism [131], as illustrated in Fig. 5.

2. m-HNTs for Pharmaceuticals, Phenolics Adsorption

Environmental pollution has long been linked to the discharge of pharmaceuticals, personal care items, phenols, and organic acids into environmental waters. Typically, petrochemicals, the cosmetics, pharmaceutical, and allied industries, as well as hospital discharges, are the main sources of these pollutants. Pharmaceuticals like antibiotics, antifungals, analgesics, and other medicines are made specifically to treat illnesses, but when their metabolites are found in water bodies, they are considered to be harmful [145]. They usually get into the water through body excretion and hospital discharge. Phenols, on the other hand, are precursors used in pharmaceuticals, dyes, herbicides, pesticides, detergents, epoxies, and other chemical processing industries [146]. It has been estimated that more than 10 million tons of phenol compounds are discharged annually into the environment, thus polluting the soil and subsequently migrating into the surface and underground waters [147,148]. Both pharmaceutical drugs metabolites and phenols are toxic when present in water bodies, even at lower concentrations of ng/L. They are persistent to natural biodegradation and, thus, are classified as priority pollutants and endocrine disruptors by USEPA and EU [133,149]. Despite various efforts made using physical and biological processes, such as membrane technologies and coagulation, these pollutants remain persistent in the environment and require more advanced technologies for remediation [150]. Adsorption has been put forward as alternative for their elimination from aqueous media.

HNTs are widely employed for organic pollutant adsorption. The physical properties of the HNTs, such as porosity, hydrophilicity (water contact angle of HNT is 10±3°), good water dispersibility as well as the chemical properties such as surface charges due to aluminol (Al-OH) and silanol (Si-OH) groups, are well utilized and devoted for pharmaceutical and phenol adsorption. Thus, Ramanayaka et al. [151] explored the use of HNT for the adsorption of antibiotic OTC. With the adsorption obeying pseudo-second order kinetic model, a maximum adsorption capacity of 52.4 mg/g was reached in 90 minutes. The adsorption was driven by the active pores of the HNTs, the array of aluminol (Al-OH) groups on the interlayer surface, and the surface of the internal lumen. Since HNTs frequently have a low affinity for active guest compounds such phenols and medicines, modification is preferred to produce site-specific HNTs with high selectivity. For instance, high temperature (600-900 °C) has been demonstrated to replace the silanol surface (Si-OH) with hydroxyl (-OH) group [152], which is prominent for attracting guest molecules with positively charged surface to form electrostatic bond. The adsorption properties of sulfuric acid modified and pristine HNTs towards aqueous removal of chloro-anilines. Acid activation was said to improve the porosity of the HNT, with BET surface area of 42.1 and 76.6 m^2/g for the pristine and modified HNTs, respectively. Thus, the latter achieved complete adsorption of the 3-CA, 4-CA within 180 min, while for

3,4-DCA, equilibrium was achieved in 360 mins. Also, their adsorption was governed by pseudo-second order model [153]. Salaa et al. [154] reported on a novel synthesis of hexadecyltrimethylammonium (HDTMA) surfactant modified HNT via intercalation method for the adsorption of diclofenac (DFC). The highest adsorption efficiency achieved was 154.3 mg/g and it was entropically endothermic and spontaneous. The interaction between the DFC and the adsorbent occurred via electrostatic interaction between the anionic DFC molecules, which was hydrophobically bonded to HDTMA tail, and positively charged lumen containing Al-OH group as depicted in Fig. 6.

The hydrophilicity of HNTs coupled with the flexibility and film-forming property of polymers such as polyethersulfone (PES) could be used to prepare mixed matrix membranes with synergetic properties for wastewater remediation. Thus, Elakkiya et al. reported on HNT decorated polyphenylsulfone/polyaniline (HNT-PANI) for the fabrication of highly stable PES/HNT-PANI membrane with antifouling and retention properties, thus achieving 95% efficiency for humic acid (HA) adsorption [146]. Hydrophobic poly (vinylidene fluoride) (PVDF) membrane has been widely employed in analytical chemistry for solid phase microextraction applications. Its surface modification with inorganic nanoparticles such as silica (SiO_2), titania (TiO_2) materials has been shown to improve the performance of the membrane for entrapment of analytes from the aqueous media. AbdulKadir et al. reported for the first time the use of PVDF-HNT membrane with water repellent property for

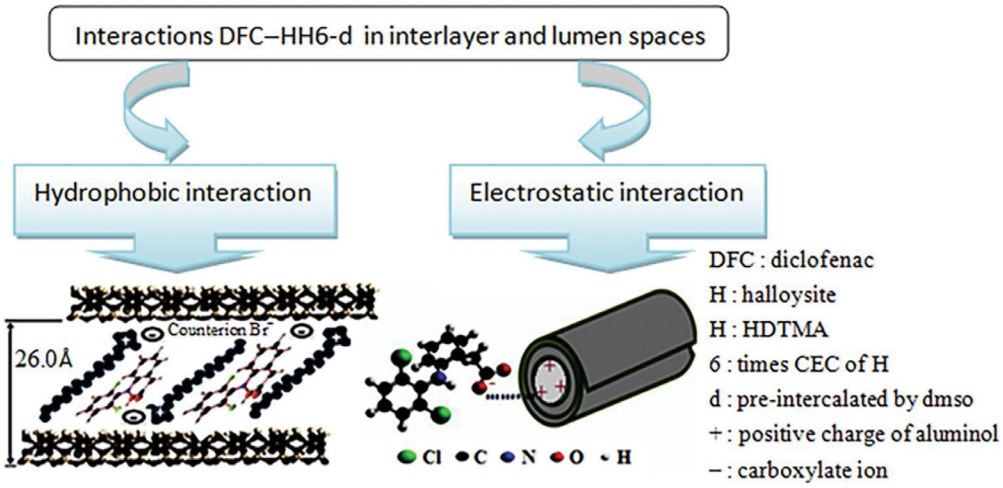

Fig. 6. Mechanism for DCF adsorption onto HNT-HDTMA composite. Reproduced from ref. [154].

Table 3. Compilation of various m-HNTs for pharmaceuticals and phenolics adsorption

Adsorbent	Pollutant	Adsorption parameters				Highlights	References
		pH	Temp (K)	Adsorbate conc (mg/L)	Contact time		
HNT In_2O_3/HNT	TC	1-7	293-353	10-50	0-60 min	The nanocomposite exhibited 4 times adsorption capacity than the pristine HNT.	[156]
HNT	OTC	3-9	303	25-173	0-1,600 min	The adsorption proceeded via chemisorption with intra-particle diffusion as the rate limiting step.	[151]
GO/HNT@PANI	DS	2-10	288-308	50-700	0-60 min	The adsorption occurred via electrostatic, hydrogen and π-π bonds and was affected by change in pH and concentration.	[157]
Ag_3PO_4-HNT	DS IBP FLP NPX	-	-	8-500	0-600 min	The higher adsorption capacity was ascribed to the HNT.	[133]
HNT HNT-PAMAM	IBP NPX	3-11	298-318	50-400	0-24 hours	Grafting the HNT with PAMAM dendrimer significantly improved the adsorption efficiency.	[158]

Table 3. Continued

Adsorbent	Pollutant	Adsorption parameters				Highlights	References
		pH	Temp (K)	Adsorbate conc (mg/L)	Contact time		
A-HNT	4-CA 3-CA 3,4-DCA	-	293	5-80	10-1,440 min	Higher adsorption efficiency of the pollutants was achieved with intra-particle diffusion at limiting step.	[153]
HNTs-PANI	HA	1-12	-	10-100	-	The membrane demonstrated higher stability for the HA adsorption.	[146]
HNT	Ani 4-CA	-	298-358	200	-	The adsorption of the pollutant onto the HNT was well described by Langmuir model.	[159]
HNT	5-ASA		298-318	225	0-24 hours	Rapid adsorption of the 5-ASA onto the external surface of the HNT was achieved.	[160]
CMC-HNTs	CAP	2-6	298-318	50-300	0-120 min	The adsorbent exhibited higher performance and good reusability.	[161]
TiO_2-HNT Fe_2O_3-HNT	2-CA 2,6-DCA	-	298	5-40	0-24 hours	The adsorption obeyed Langmuir model with the adsorbent having multiple active sites.	[149]
HNT HNT/HDTMA HNT/HDTMA/CEC	DFC	6-12	298-328	20-300	0-120 min	Ease of regeneration and higher adsorption efficiency was achieved.	[154]
HNT HNT/Alginate	TC	2.8-8.5	-	25-150	0-1,440 min	The adsorption of TC on both HNT and composite was improved at higher pH and was well fitted by pseudo-second order model.	[80]
CTs-HNT	Ph	4-10	298	-	0-200 min	The biohybrid material exhibited good stability and efficiency for phenol adsorption.	[162]
HNT Cu^{2+}-HNT	2,4,6-TCP	3-10	-	25-200	0-24 hours	The nanocomposite has shown higher adsorption efficiency than the pristine HNT due to the surface area enhancement.	[163]
HNT	TC CAP	2-12	298-318	25-200	0-600 min	The activation of the HNT improved its surface area and adsorption efficiency.	[164]
HNT	OFL	1.2-7.4	-	100	0-24 hours	The NaOH activation of the HNT improved its surface area for ofloxacin adsorption.	[117]
HNT	Cip	2-10	-	0-50	0-300 min	HNT demonstrated the best adsorption capacity among the various clay minerals employed.	[165]

oxytetracycline adsorption [155]. The incorporation of the HNT was found to improve the permeate flux of the membrane at both lower and higher concentrations, thus achieving 100% adsorption of OTC at 100 mg/L concentration. The overall mechanism for the adsorption was correlated with chemical interaction, electrostatic force, and pore interaction. The predominant was the chemical interaction between the F atom from the PVDF and the hydroxyl group (-OH) of OTC, resulting in the formation hydrogen bonding (F—H-O) [155]. Table 3 presents the adsorption of pharmaceuticals and phenolics onto various m-HNTs and HNT membranes reported in the literature.

3. m-HNTs for Heavy Metals and Metal Ions Adsorption

The presence of heavy metals in environmental waters due to human activity and untreated industrial effluent discharge, and

poor sewage disposal policies has been known to cause serious deterioration to the ecosystem. They are a group of inorganic chemical species that are released from industries such as tannery, electroplating, metal finishing, nuclear power, and mining sites. [76]. They are highly mobile and non-biodegradable elements; thus, they can be transported from the various sources such as soil, landfills, and leachate into environmental waters. They are harmful to both flora and fauna and have detrimental effects on aquatic organisms [166]. They accumulate in the surface water and can be easily transmitted through the food chain into the humans and animals, causing severe ailments, such as kidney and liver damage, brain and skin cancer, anemia, pneumonia, hemoglobinuria, gastric dysfunction, diarrhea, and vomiting [167,168]. Due to their toxicity, the E.U and USEPA have listed them among the carcinogenic substances of priority concerned, which requires immediate elimination [47]. Thus, various methods are employed for their remediation including physical, biological, and chemical treatments. Adsorption, being one of the most prosperous, has been well explored for heavy metals remediation.

Clay minerals are well utilized for heavy metal adsorption and the HNTs are famous for such applications [101,169]. It plays significant role for their elimination due to the charge interaction between the hydroxyl group (-OH) of the HNTs and the positively charged metals species such as Pb^{2+}, Cr^{4+}, Ni^{2+}, Fe^{2+}, Na^{+} etc. The use of fine grained HNT for the adsorption of Pb^{2+} and Cu^{2+} was reported with the adsorbent achieving over 95% efficiency [170]. The adsorption of Pb^{2+} onto magnetic HNT (MHNT) and Mn_2O_3 deposited MHNT synthesized via hydrothermal method was employed by Afzali and Fayazi [171]. Excellent performance of the two adsorbents was observed with equilibrium achieved within 60 mins. The Mn_2O_3 coating greatly influenced the performance of the composite by improving the surface area, pore size and electrochemical property of the adsorbent; thus, the adsorption capacity was 11 and 39 mg/g for MHNT and MNHT@Mn_2O_3, respectively. The MNHT@Mn_2O_3 was also prominent for effective reusability, achieving over 90% efficiency for five consecutive cycles [171]. Copper nanocluster HNT composite (CuNCs@HNT) was also employed for Cr^{4+} adsorption [172]. The porosity of the CuNCs@HNT composite decreased in comparison to the pristine HNT with the BET surface area of 47.23 and 24.61 m^2/g for the latter and the former, respectively, attributed to the clogging of the HNT pores by the CuNCs. However, the pore diameter increased from 6.17 to 10.44 nm for the HNT and CuNCs@HNT, respectively. The presence of the CuNCs in the resulting in the multifunctional property of the composite and significantly enhanced its adsorption by facilitating the reduction of Cr^{4+} to Cr^{3+}, which binds to the HNT surface via electrostatic attraction, thus achieving adsorption capacity of 80 mg/g at pH 5 [172].

HNT membranes have also exhibited good performance for heavy metals and metal ions adsorption. For example, amino grafted membrane of HNT blended chitosan-poly vinyl alcohol (CT/PVA) fabricated via electrospinning was employed for the heavy metal adsorption. The CS/PVA/HNT-NH_2 membrane exhibited good crystallinity and thermal stability and tensile strength. Thus, it has shown good performance for the adsorption of Pb^{2+} and Cd^{2+} uptake [173]. The affinity of the membrane to the heavy metals

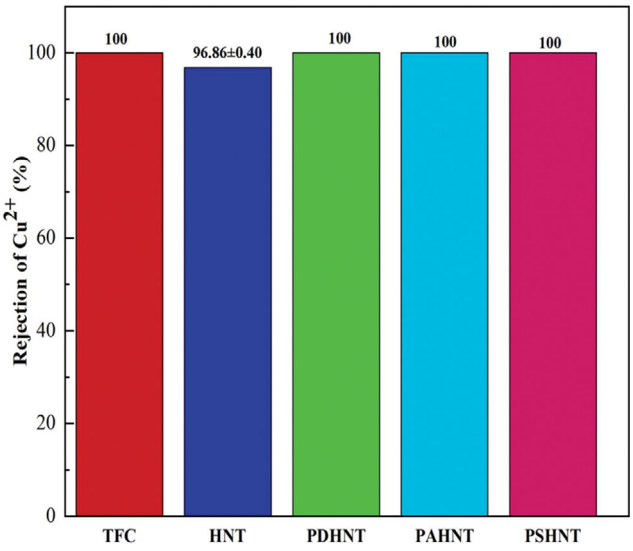

Fig. 7. HNT membrane with different polymers for Cu^{2+} adsorption (TFC=Thin film composite, PHHNT=HNT coated with polydopamine, PAHNT=HNT coated with polyaniline, PSHNT= HNT coated with polystyrene). Reproduced from ref. [174].

increased with the HNT-NH_2 content, attributed to the NH_2 functionalization, with the adsorbate uptake increased from 40 to 65 mg/g for Pb^{2+} adsorption. Similarly, combining the porosity of the CS/PVA to the HNT-NH_2 capacity improved the performance of the membrane, achieving maximum adsorption capacity of 457.5 and 476.2 mg/g for Pb^{2+} and Cd^{2+}, respectively, using initial concentrations of 450 mg/L. The stability of the membrane was also utilized for good reusability up to five consecutive cycles [173]. Most recently Fallahnejad et al. [174] reported on the fabrication of HNT membrane coated with different polymers: polydopamine (PDHNT), polyaniline (PHNT) and polystyrene (PSHNT) for metal ions adsorption. The hydrophilic property of the polymers intensified permeation fluxes of the membrane and its adsorption performance, achieving complete adsorption of Cu^{2+} as shown in Fig. 7. Similarly, a functionalized 3-aminopropyltriethoxysilane (APTES) and polyvinylidene fluoride (PVDF) HNT membrane (A-HNT@PVDF) was fabricated by Zeng et al. [142] for the adsorption of heavy metals and dyes adsorption. The hydrophilicity of the membrane was reflected in efficient performance and reusability towards heavy metals uptake. Thus, complete adsorption of Cu^{2+} was recorded as pH 5.5, attributed to the enhancement in the charge interaction between the negatively charged A-HNT surface and the positively charged Cu^{2+} [142]. The effective adsorption of heavy metals onto various HNTs is highlighted in Table 4.

4. m-HNTs for the Removal of Anionic Species

Due to their high reactivity, some of the heavy metal pollutants occur in wastewater or surrounding water in the form of anionic species [175]. Typical examples are chromate [24], arsenite [176], arsenate [177] etc. Removal of these anionic species is often achieved through surface complexation using the negative charges on their surface, which binds with positive charge or substitute another negative from the adsorbent surface [178]. Song et al. [176] used

Table 4. Compilation of various HNTs for heavy metals and metal ions adsorption

Adsorbent	Pollutant	Adsorption parameters				Highlights	References
		pH	Temp (K)	Adsorbate conc (mg/L)	Contact time		
RGO/HNT	Cu^{2+} Cr^{3+}	2-12	293-313	50	20-120 min	The membrane has shown great potential even after several uses.	[49]
Hal/Fe_2O_3/ CS/PEO	Cr^{3+} Cd^{2+} Cu^{2+} Pb^{2+}	3-7	298	100	0-160 min	The adsorption occurred on the heterogenous surface of the membrane.	[184]
HNT@PDA	U^{4+}	3-10	298-328	10-100	0-8 hours	HNT@PDA composite demonstrated better adsorption efficiency than the pristine HNT for repeated cycles.	[81]
A-HNT@PVDF	Cu^{2+} Cd^{2+} Cr^{6+}	3-11	-	5	30-180 min	The membrane more effectively removed the heavy metals than the pure PVDF.	[142]
PPy-HNT	Cr^{4+}	2-11	283-318	25-100	0-600 min	The adsorbent can remove heavy metal effectively even in the presence of co-existing ions.	[185]
CS/PVA/ HNT-NH_2	Pb^{2+} Cd^{2+}	1-7.5	283-318	50-1,000	0-360 min	The functionalization of the HNT greatly improved the adsorption capacity.	[173]
Na-HNT/ HDTMA	Cr^{4+}	3-10	283	25-300	0-240 min	The adsorption efficiency of the composite was reduced by increasing pH and ionic strength.	[186]
CuNCs@HNT	Cr^{4+}	3-10	283	1-100	0-48 hours	The composite showed good stability for repeated number of adsorption cycles.	[172]
PSHNT	Cu^{2+} Na^{+}	-	-	200-500	1 hour	The membrane was characterized by higher uptake of the analytes.	[174]
HNT HNT/Fly ash	Fe^{3+} Mn^{2+} Cu^{2+} Zn^{2+} Ni^{2+} Pb^{2+}	5.5	-	0.03-0.86	-	The membrane effectively adsorbed the heavy metals using the biofilter system.	[170]
C-HNTs	Zn^{2+}	-	283	1.0-9.0 $\times 10^{-6}$ M	30 min	The coumarin-anchored HNT selectively adsorbed the Zn^{2+} with higher efficiency.	[187]
HNT HNT-NH_2	Pb^{2+}	3-6	283	30	0-240 min	The adsorption efficiency of both pristine and functionalized HNT increased at lower pH and ionic strength.	[188]
Fe_2O_3-HNT/ biochar	Pb^{2+} Cu^{2+} Zn^{2+} Cr^{4+}	2-6	283	100-500	1-1,440 min	The magnetic adsorbent exhibited good regeneration performance with the adsorption proceeded via monolayer chemisorption process.	[189]
HNT-bent/mag	Cr^{4+}	1-10		50-600	0-60 min	The nanocomposite exhibited higher adsorption efficiency.	[76]

HNT-CeO_2 composite to remove As(III) in aqueous solution, and discovered that As(III) has strong interaction with cerium of the adsorbent through Ce-O-As surface complex formation and through partial oxidation of As(III) to As(V) by the Ce(IV). Similarly, polyethylenimine modified HNT adsorbent was discovered to be highly efficient in the removal of chromate at low pH, and this was ascribed to the electrostatic interaction between the ammonium ion (formed at low pH) of the polyethylenimine modified HNT and the negative charge of the chromate ion [24]. Additionally, the hydrogen in the ammonium ion can undergo hydrogen bonding with the oxygen of chromate ion. Earlier, Jinhua et al. had immobilized quaternary ammonium ions on HNT surface through hexadecyltrimethyl-

Table 4. Continued

Adsorbent	Pollutant	Adsorption parameters				Highlights	References
		pH	Temp (K)	Adsorbate conc (mg/L)	Contact time		
HNT Amine-HNT	Pb^{2+} Cd^{2+} Zn^{2+} Cu^{2+}	2-7	282	0.005-5.0 mmol/L	0-20 min	The amine group aided the diffusion of the pollutants to the active site of the adsorbent, hence its higher adsorption efficiency.	[190]
HNT	Ag^{2+}	4-6	293-323	50-110	0-120 min	The adsorption was best described as pseudo-second order governed by monolayer coverage.	[132]
MHNTs@MnO_2	Pb^{2+}	2-8	298-328	50	0-200 min	The adsorption capacity of the composite is high, and the rate is fast for the removal of Pb^{2+}.	[171]
HNT	NH^{4+}	2-11	288-313	10-600	10-120 min	The adsorption became saturated at higher concentration.	[191]
HNT HNTs-(DEN-NH_2)	Cr^{4+}	2-7	298-328	3-11	0-60 min	The HNT composite has shown higher adsorption efficiency via monolayer formation.	[192]
HNT HNT/CH_3-COONa	Cu^{2+}	2-6	298-328	1,000-2,500	0-240 min	The intercalation of the HNT by CH_3COONa improved the adsorption performance.	[193]
HNT/Alginate	Pb^{2+}	5	-	0-200	0-24 hours	Both HNT and alginate have contributed to the high uptake of the Pb^{2+}.	[194]
Ca-HNT	Fe^{2+}	4-10	293-323	5-100	5-80 min	The adsorption efficiency of the adsorbent decreased as the initial concentration of Fe^{2+} increased.	[195]
$NiFe_2O_4$/HNTs/GQDs	Pb^{2+}	3-6	288-388	10-100	10-60 min	The higher efficiency of the adsorbent was ascribed to the complexation interaction of the functional groups and the Pb^{2+}.	[196]
HNT Magnetic HNT	Ag^{2+}	-	-	1-200	0-3 hours	The magnetic HNT allowed for easy separation of the Ag^{2+}.	[197]
CT/HNT	Cu^{2+}	-	298-300	100	0-12 hours	The NH_2 and -OH from chitosan and HNT facilitated adsorption.	[198]
Fe_3O_4/HNTs	As^{3+} As^{4+}	4-10	293-313	0.1-300	15-1,440 min	The magnetic adsorbent allows for better performance and easy regeneration.	[199]
HNT@GO	U^{4+}	2-10	298-338	-	0-24 hours	The adsorbent exhibited both properties of GO and HNT.	[200]

ammonium bromide grafting, which adsorbs chromate ions via electrostatic interaction [179]. Electron-rich polypyrrole coated HNT, prepared by in situ oxidative polymerization of pyrrole in dispersed HNT solution, utilizes the electron density of polypyrrole to reduce the adsorbed chromate on the surface of the positively charged surface of HNT at low pH [180].

5. m-HNTs for Oily Water Remediation

Rapid growth of oil and gas industries due to high demand for fuel by heavy and light industries worldwide as well as vehicles consumption has had a serious effect on water bodies [181]. Offshore petroleum exploration and underground oil seep have been recognized as the primary source of the oil in oceans and seas. Petroleum refining consumes large amounts of water which is often discharged as effluents into the water bodies, thus increasing the level concentration of oil in the water [182]. Apart from that, leakage due to petroleum and petrochemical transportation by merchant ships, oil tankers, vessels, etc., is also identified as major source of oily wastewater [183].

It was reported that about 5-30 million tons of oil spills into the ocean are due to either accidents or activities of oil tankers [201]. Coal constitutes a mixture of organic and inorganic compounds and is processed for electricity generation and chemical synthesis (such as gasoline, ammonia, and urea). It has been identified as another means of oil gets into environmental waters [202]. Petro-

chemical production also contributes to the presence of oil in the water. When oil leaks into the water, it is widely transported to a longer distance due to its high polarity. Oily wastewater has been characterized as a major source of environmental pollution due to its chemical composition, comprising various toxic organic and inorganic species such as PAHs, phenols, heavy metals, and other organic and inorganic species [163,203]. Usually, the oil acts as surfactant, occupying the surface of the water and consequently blocking the supply of oxygen demanded for the respiration of aquatic organisms.

The obligation for the separation of oil/water mixture has been recognized and clay materials have also been investigated. HNTs have been utilized for such applications. A work was reported on the fabrication of facile and eco-friendly ultrafiltration mixed matrix membrane for oily wastewater remediation. The membrane was synthesized by incorporating HNT-hydrous ferric oxide (HNT-HFO) into polyethersulfone (PES). Increase in the HNT-HFO nanocomposite loading improved water flux and hydrophilicity of the membrane, leading to complete elimination of the oil molecules with rejection efficiency of 99.7% [204]. Additionally, ZnO-HNT improved the properties of the membrane by enhancing its hydrophilicity, antifouling and oil rejection capacity. In comparison to the pristine, the modified membrane achieved higher oil-water separation (with 99% efficiency), attributed to the excellent water permeation flux of the membrane due to the availability of -OH groups and agglomeration of ZnO-HNT on its surface [205]. A novel ultra-membrane prepared by incorporation of 3-Aminopropyltriethoxysilane-grafted HNT (APTES-HNT) into PVDF was also reported by Zheng et al. for the separation of oil/water emulsions. The oil-rejection performance of the APTES-HNT/PVDF membrane was over 90% with 82.9% antifouling efficiency achieved after three consecutive cycles [206]. Similar membrane with super hydrophilic property was fabricated by Wang et al. by incorporating HNT and graphene on the surface of the PVDF. The separation efficiency of the membrane was 99.5% with high pure water flux of 1,500 $L/m^2/h$ [207]. The HNTs on the surface of the membrane prevented the aggregation of the oil droplets and allowed it to settle below the aqueous layer, thereby improving separation efficiency.

CHALLENGES FOR m-HNTs ADSORBENTS AND FUTURE PERSPECTIVES

m-HNTS as adsorbents were proven to be very good in the removal of dyes, pharmaceuticals and heavy metals from wastewater; however, there is need for more tests which should include other contaminants such as phenolic compounds, pesticides, herbicides, pharmaceuticals, oil and grease (O & G), anionic species as well as micro pollutants. Furthermore, because m-HNTs are yet to be used as commercial adsorbents, researchers will need to focus their efforts on developing more efficient adsorbents for industrial usage. Also, the adsorption mechanisms of m-HNTs and the interactions between structure, surface character, and adsorptive activity have not been well explored. Many researchers use synthetic wastewater for adsorption experiments; therefore, testing m-HNTs as adsorbents in a more realistic environment, such as real wastewater containing various contaminants, is critical. Another factor to consider is that most researchers overlook the adsorbents' lifecycles; therefore, investigating adsorption/desorption cycles is highly suggested. Other critical challenges that must be addressed include the proper disposal of polluted adsorbents and the cost of producing customized adsorbents for specific uses. There is also the need for future work to focus on reducing the mobility of various pollutants in soil environments by studying the application of these m-HNTs as adsorbents in pilot scale processes as well as soil amendments. There are still many challenges, such as lacking sufficient stability towards long-term applications and instability that also need addressing despite the significant progress achieved in m-HNTs structures. These weaknesses could become a roadblock in the future when it comes to commercializing the usage of HNTs. To keep up with the fast-rising efforts on their synthesis and characteristics for various applications, more devotion to improving stability (such as photostability, thermal stability, moisture stability, and chemical stability) is required.

CONCLUSIONS

This has been a comprehensive literature overview on the potential of m-HNTs as adsorbents. The focus was on the application of the m-HNTs as adsorbents for the removal of dyes, heavy metals, anionic species as well as purifying oily wastewater. The success of m-HNTs as adsorbents is owing to their excellent biocompatibility renewability, economic value, non-toxicity, high mechanical properties and surface area. Upon comparison with other adsorbents, m-HNTs proved to be very good in removing pharmaceuticals, dyes and heavy metals, so their application needs to be expanded so that they can cover other water and wastewater contaminants. Given the current engineering practice of "reduce, reuse, and recycle," materials with HNT features may attract more study interest and, as a result of their potential, become the next promising materials of the future.

LIST OF ABBREVIATIONS

Abbreviation

4-NP : 4-nitrophenol
APTES : aminopropyltriethoxysilane
BET : Brunauer-Emmett-Teller
BJH : Barrett-Joyner-Halenda
CA : chloro-anilines
CNTs : carbon nanotubes
e^- : electron
EDX : energy dispersive X-Ray analysis
EU : european union
FTIR : fourier transform infrared spectroscopy
GO : graphene oxide
h^+ : holes
HA : humic acid
HDTMA : hexadecyltrimethylammonium
HNTs : halloysite nanotubes
ICDD : international centre for diffraction data
ICP-OES : inductively coupled plasma atomic emission spectroscopy

MB : methylene blue
m-HNTs : modified halloysite nanotubes
MO : methyl orange
Nm : nanometer
PANI : polyaniline
PD : polydopamine
PE : polyelectrolytes
PEG : polyethylene glycol
PEI : polyethyleneimine
PES : polyethersulfone
PVA : polyvinyl alcohol
PVDF : polyvinylidene fluoride
RhB : Rhodamine B
SA : succinic acid anhydride
SDGs : sustainable development goals
SEM : scanning electron microscope
SERS : surface-enhanced Raman spectroscopy
TA : tannic acid
TEM : transmission electron microscopy
TEPA : tetraethylenepentamine
TGA : thermogravimetric analysis
TOC : total organic carbon
TPR : temperature-programmed reduction
USEPA : united state environmental protection authority
XRD : X-ray diffraction
XRF : X-ray fluorescence

DECLARATION OF COMPETING INTEREST

The authors declare that they have no known competing financial interests or personal relationships that could have appeared to influence the work reported in this paper.

REFERENCES

1. A. M. Nasir, J. Jaafar, F. Aziz, N. Yusof, W. N. W. Salleh, A. F. Ismail and M. Aziz, *J. Water Proc. Eng*., **36**, 101300 (2020).
2. M. Ahmaruzzaman, *Mater. Res. Bull*., **140**, 111262 (2021).
3. F. Cai, L. Lei, Y. Li and Y. Chen, *Sci. Total Environ*., **782**, 146852 (2021).
4. Y. Wu, H. Ye, C. You, W. Zhou, J. Chen, W. Xiao, Z. N. Garba, L. Wang and Z. Yuan, *Sep. Purif. Technol*., **285**, 120301 (2021).
5. J. Meza-González, M. Hernández-Quiróz, F. Rojo-Callejas, E. Hjort-Colunga, M. Mazari-Hiriart, E. Valiente-Riveros, O. Arellano-Aguilar and C. Ponce de León-Hill, *Bull. Environ. Cont. Toxicol*., **108**, 114 (2022).
6. W. Colglazier, *Science*, **349**, 1048 (2015).
7. D. Kanakaraju, B. D. Glass and M. Oelgemöller, *J. Environ. Manage*., **219**, 189 (2018).
8. I. Levchuk, J. J. Rueda Márquez and M. Sillanpää, *Chemosphere*, **192**, 90 (2018).
9. S. Verma, A. Daverey and A. Sharma, *Environ. Technol. Rev*., **6**, 47 (2017).
10. A. A. Adetokun, S. Uba and Z. N. Garba, *J. King Saud Univ. - Sci*., **31**, 1452 (2019).
11. A. R. Afidah and Z. N. Garba, *J. Assoc. Arab Universities Basic Appl. Sci*., **21**, 17 (2016).
12. W. Zhou, H. Ye, Z. Zhong, Q. Lu, R. Liu, M. Zhang, Z. N. Garba, L. Wang and Z. Yuan, *Cellulose*, **28**, 9893 (2021).
13. B. Rezai and E. Allahkarami, *Soft Computing Techniques in Solid Waste and Wastewater Management*, 35 (2021).
14. R. Selvasembian, W. Gwenzi, N. Chaukura and S. Mthembu, *J. Hazard. Mater*., **417**, 125960 (2021).
15. M. H. Hussin, N. A. Pohan, Z. N. Garba, M. J. Kassim, A. R. Afidah, N. Brosse, M. Yemloul, M. R. N. Fazita and M. K. M. Haafiz, *Intl. J. Biol. Macromol*., **92**, 11 (2016).
16. B. Rezai and E. Allahkarami, *Soft Computing Techniques in Solid Waste and Wastewater Management*, 75 (2021).
17. W. Li, B. Mu and Y. Yang, *Bioresour. Technol*., **277**, 157 (2019).
18. K. Maru, S. Kalla and R. Jangir, *New J. Chem*., **46**, 3054 (2022).
19. A. Gupta, V. Sharma, K. Sharma, V. Kumar, S. Choudhary, P. Mankotia, B. Kumar, H. Mishra, A. Moulick, A. Ekielski and P. K. Mishra, *Materials*, **14**, 4702 (2021).
20. S. Marković, A. Stanković, Z. Lopičić, S. Lazarević, M. Stojanović and D. Uskoković, *J. Environ. Chem. Eng*., **3**, 716 (2015).
21. B. Kumar, K. Smita, E. Sánchez, C. Stael and L. Cumbal, *Ecol. Eng*., **93**, 152 (2016).
22. E. Allahkarami, A. D. Monfared, L. P. O. Silva and G. L. Dotto, *Sci. Rep*., **12**, 10718 (2022).
23. P. Santander, B. Butter, E. Oyarce, M. Yáñez, L. P. Xiao and J. Sánchez, *Ind. Crop Prod*., **167**, 113510 (2021).
24. X. Tian, W. Wang, Y. Wang, S. Komarneni and C. Yang, *Micropor. Mesopor. Mater*., **207**, 46 (2015).
25. Z. N. Garba, W. Zhou, I. Lawan, M. Zhang and Z. Yuan, *Cellulose*, **26**, 6241 (2019).
26. M. Irannajad and H. Kamran Haghighi, *Environ. Processes*, **8**, 7 (2021).
27. Z. N. Garba and A. R. Afidah, Penang, Malaysia, 170 (2014).
28. Z. N. Garba, A. R. Afidah and S. A. Hamza, *J. Environ. Chem. Eng*., **2**, 1423 (2014).
29. Z. N. Garba, F. B. S. Shikin and A. R. Afidah, *J. Chem. Eng. Chem. Res*., **2**, 623 (2015).
30. F. García-Araya, F. J. Beltrán, P. Álvarez and F. J. Masa, *Adsorption*, **9**, 107 (2003).
31. O. Gercel, A. Ozcan and S. Ozcan, *Appl. Surf. Sci*., **253**, 4843 (2007).
32. M. Goncalves, M. C. Guerreiro, L. C. A. Oliveira, C. Solar, M. Nazarro and K. Sapag, *Waste Biom. Valor*., **4**, 395 (2013).
33. P. González-García, *Renew. Sustain. Energy Rev*., **82**, 1393 (2018).
34. A. Amari, F. M. Alzahrani, K. M. Katubi, N. S. Alsaiari, M. A. Tahoon and F. B. Rebah, *Materials*, **14**, 1365 (2021).
35. F. Karimi, A. Ayati, B. Tanhaei, A. L. Sanati, S. Afshar, A. Kardan, Z. Dabirifar and C. Karaman, *Environ. Res*., **203**, 111753 (2022).
36. T. A. Saleh, *Environ. Technol. Innov*., **24**, 101821 (2021).
37. E. Allahkarami and B. Rezai, *Proc. Saf. Environ. Protect*., **124**, 345 (2019).
38. M. Hasanpour and M. Hatami, *Adv. Colloid Interface Sci*., **284**, 102247 (2020).
39. M. Fizir, A. Richa, H. He, S. Touil, M. Brada and L. Fizir, *Rev. Environ. Sci. Biotechnol*., **19**, 241 (2020).
40. M. Ghanbari, D. Emadzadeh, W. J. Lau, S. O. Lai, T. Matsuura and A. F. Ismail, *Desalination*, **358**, 33 (2015).
41. M. Massaro, M. Casiello, L. D'Accolti, G. Lazzara, A. Nacci, G.

Nicotra, R. Noto, A. Pettignano, C. Spinella and S. Riela, *Appl. Clay Sci.*, **189**, 105527 (2020).
42. A. Glotov, A. Vutolkina, A. Pimerzin, V. Vinokurov and Y. Lvov, *Chem. Soc. Rev.*, **50**, 9240 (2021).
43. R. Gusain, N. Kumar and S. S. Ray, *Coord. Chem. Rev.*, **405**, 213111 (2020).
44. W. Ma, H. Wu, Y. Higaki and A. Takahara, *Chem. Rec.*, **18**, 986 (2018).
45. L. Yu, H. Wang, Y. Zhang, B. Zhang and J. Liu, *Environ. Sci: Nano*, **3**, 28 (2016).
46. M. Liu, Z. Jia, D. Jia and C. Zhou, *Prog. Polym. Sci.*, **39**, 1498 (2014).
47. I. Anastopoulos, A. Mittal, M. Usman, J. Mittal, G. Yu, A. Núñez-Delgado and M. Kornaros, *J. Mol. Liq.*, **269**, 855 (2018).
48. A. Grylewicz and S. Mozia, *Sep. Purif. Technol.*, **256**, 117827 (2021).
49. Y. Liu, W. Tu, M. Chen, L. Ma, B. Yang, Q. Liang and Y. Chen, *Chem. Eng. J.*, **336**, 263 (2018).
50. A. Haruna, I. Abdulkadir and S. O. Idris, *J. King Saud Univ. - Sci.*, **32**, 896 (2020).
51. A. Haruna, I. Abdulkadir and S. O. Idris, *Heliyon*, **6**, e03237 (2020).
52. Z. N. Garba, W. Xiao, W. Zhou, I. Lawan, Y. Jiang, M. Zhang and Z. Yuan, *Korean J. Chem. Eng.*, **36**, 1826 (2019).
53. Z. N. Garba, W. Zhou, M. Zhang and Z. Yuan, *Chemosphere*, **244**, 125474 (2020).
54. Y. Lvov, W. Wang, L. Zhang and R. Fakhrullin, *Adv. Mater.*, **28**, 1227 (2016).
55. J. Kurczewska, P. Pecyna, M. Ratajczak, M. Gajęcka and G. Schroeder, *Saudi Pharm. J.*, **25**, 911 (2017).
56. Q. Li, T. Ren, P. Perkins, X. Hu and X. Wang, *Food Control*, **124**, 101876 (2021).
57. S. Saadat, G. Pandey, M. Tharmavaram, V. Braganza and D. Rawtani, *Adv. Colloid Interface Sci.*, **275**, 102063 (2020).
58. H. Wu, M. Li, Y. Zhao, Z. Zhou, S. Hua and J. Zhang, *Chem. Eng. Res. Des.*, **180**, 55 (2022).
59. C. S. C. Chiew, W. Gourich, P. Pasbakhsh, P. E. Poh, B. T. Tey, C. P. Song and E. S. Chan, *J. Water Proc. Eng.*, **45**, 102531 (2022).
60. T. Ngulube, J. R. Gumbo, V. Masindi and A. Maity, *J. Mol. Struct.*, **1184**, 389 (2019).
61. M. Xie, K. Huang, F. Yang, R. Wang, L. Han, H. Yu, Z. Ye and F. Wu, *Int. J. Biol. Macromol.*, **151**, 1116 (2020).
62. A. M. Alakrach, A. A. Al-Rashdi, T. Alqadi, M. A. Alsaadi, S. S. Ting, O. S. Dahham and N. N. Zulkepli, *Mater. Sci. Forum*, **102**, 270 (2021).
63. D. Wu, J. Li, J. Guan, C. Liu, X. Zhao, Z. Zhu, C. Ma, P. Huo, C. Li and Y. Yan, *J. Ind. Eng. Chem.*, **64**, 206 (2018).
64. F. Liu, L. Bai, H. Zhang, H. Song, L. Hu, Y. Wu and X. Ba, *ACS Appl. Mater. Interfaces*, **9**, 31626 (2017).
65. T. Teymourian, M. R. Alavi Moghaddam and E. Kowsari, *Environ. Sci. Pollut. Res.*, **29**, 9124 (2022).
66. S. Kouser, S. Sheik, G. K. Nagaraja, A. Prabhu, K. Prashantha, J. N. D'souza, K. M. Navada and D. J. Manasa, *Int. J. Biol. Macromol.*, **165**, 1079 (2020).
67. E. Nyankson, B. Agyei-Tuffour, J. Adjasoo, A. Ebenezer, D. Dodoo-Arhin, A. Yaya, B. Mensah and J. K. Efavi, *Adv. Mater. Sci. Eng.*, **2019**, 4270310 (2019).
68. C. E. Tas, S. Hendessi, M. Baysal, S. Unal, F. C. Cebeci, Y. Z. Menceloglu and H. Unal, *Food Bioproc. Technol.*, **10**, 789 (2017).
69. B. Huang, M. Liu, Z. Long, Y. Shen and C. Zhou, *Mater. Sci. Eng. C*, **70**, 303 (2017).
70. K. C. Christoforidis, M. Melchionna, T. Montini, D. Papoulis, E. Stathatos, S. Zafeiratos, E. Kordouli and P. Fornasiero, *RSC Adv.*, **6**, 86617 (2016).
71. P. Yao, S. Zhong and Z. Shen, *Int. J. Photoenerg.*, **5**, 1 (2015).
72. Z. L. Cheng and W. Sun, *J. Mater. Eng. Perf.*, **24**, 4090 (2015).
73. X. Li, C. Yao, X. Lu, Z. Hu, Y. Yin and C. Ni, *Appl. Clay Sci.*, **104**, 74 (2015).
74. L. Jiang, C. Zhang, J. Wei, W. Tjiu, J. Pan, Y. Chen and T. Liu, *Chem. Res. Chinese Univ.*, **30**, 971 (2014).
75. Y. Wei, X. Liang, H. Wu, J. Cen and Y. Ji, *Appl. Clay Sci.*, **213**, 106232 (2021).
76. V. Masindi, S. Foteinis, M. Tekere and M. M. Ramakokovhu, *Mater. Today, Proc.*, **38**, 1088 (2021).
77. V. B. Yadav, R. Gadi and S. Kalra, *J. Environ. Manage.*, **232**, 803 (2019).
78. E. Türkeş and Y. Sağ Açıkel, *Int. J. Environ. Sci. Technol.*, **17**, 1281 (2020).
79. J. Lee, S. Seong, S. Jin, Y. Jeong and J. Noh, *J. Ind. Eng. Chem.*, **100**, 126 (2021).
80. S. Erdem, M. Öztekin and Y. Sağ Açıkel, *Environ. Nanotechnol. Monit. Manage.*, **16**, 100576 (2021).
81. T. Ou, Y. Wu, W. Han, L. Kong, G. Song and D. Chen, *J. Hazard. Mater.*, **424**, 127208 (2022).
82. X. Song, Y. Wang, L. Zhou, X. Luo and J. Liu, *Chem. Eng. Res. Des.*, **165**, 298 (2021).
83. G. Viscusi, E. Lamberti and G. Gorrasi, *Colloid Surf. A Physicochem. Eng. Asp.*, **633**, 127925 (2022).
84. M. Gonon, *Encyclop. Mater.: Technical Ceram. Glass.*, 560 (2021).
85. Y. Xie, Y. Zhang, J. Ouyang and H. Yang, *Phys. Chem. Miner.*, **41**, 497 (2014).
86. C. Zhou, T. Sun, Q. Gao, A. Alshameri, P. Zhu, H. Wang, X. Qiu, Y. Ma and C. Yan, *J. Taiwan Inst. Chem. Eng.*, **45**, 1073 (2014).
87. H. Chen, H. Yan, Z. Pei, J. Wu, R. Li, Y. Jin and J. Zhao, *Appl. Surf. Sci.*, **347**, 769 (2015).
88. S. Sahnoun, M. Boutahala, H. Zaghouane-Boudiaf and L. Zerroual, *New Pub: Balab.*, **57**, 15941 (2015).
89. X. Wu, C. Liu, H. Qi, X. Zhang, J. Dai, Q. Zhang, L. Zhang, Y. Wu and X. Peng, *Appl. Clay. Sci.*, **119**, 284 (2016).
90. D. Garcia-Garcia, J. M. Ferri, L. Ripoll, M. Hidalgo, J. Lopez-Martinez and R. Balart, *Appl. Surf. Sci.*, **422**, 616 (2017).
91. S. Saklar and A. Yorukoglu, *Physicochem. Probl. Miner. Process.*, **51**, 83 (2015).
92. Q. Wang, J. Zhang, Y. Zheng and A. Wang, *Coll. Surf. B: Biointerf.*, **113**, 51 (2014).
93. K. Belkassa, F. Bessaha, K. Marouf-khelifa, I. Batonneau-gener, J. Comparot and A. Khelifa, *Colloids Surf. A Physicochem. Eng. Asp.*, **421**, 26 (2013).
94. E. Abdullayev, A. Joshi, W. Wei, Y. Zhao and Y. Lvov, *ACS Nano*, **6**, 7216 (2012).
95. J. M. Falcón, T. Sawczen and I. V. Aoki, *Front. Mater.*, **2**, 69 (2015).
96. C. Cheng, W. Song, Q. Zhao and H. Zhang, *Nanotechnol. Rev.*, **9**, 323 (2020).
97. M. Ayiania, E. Weiss-Hortala, M. Smith, J. S. McEwen and M. Garcia-Perez, *Carbon*, **167**, 559 (2020).

98. X. He, X. Liu, B. Nie and D. Song, *Fuel*, **206**, 555 (2017).
99. H. Krüger, V. Kahlenberg and R. Kaindl, *J. Solid State Chem.*, **180**, 922 (2007).
100. B. Zsirka, E. Horváth, P. Szabó, T. Juzsakova, R. K. Szilágyi, D. Fertig, É. Makó, T. Varga, Z. Kónya, Á. Kukovecz and J. Kristóf, *Appl. Surf. Sci.*, **399**, 245 (2017).
101. N. Danyliuk, J. Tomaszewska and T. Tatarchuk, *J. Mol. Liq.*, **309**, 113077 (2020).
102. J. Feng, H. Fan, D. A. Zha, L. Wang and Z. Jin, *Langmuir*, **32**, 10377 (2016).
103. R. L. Frost, *Clays Clay Miner.*, **43**, 191 (1995).
104. W. O. Yah, A. Takahara and Y. M. Lvov, *J. Am. Chem. Soc.*, **134**, 1853 (2012).
105. T. Ormanci-Acar, F. Celebi, B. Keskin, O. Mutlu-Salmanlı, M. Agtas, T. Turken, A. Tufani, D. Y. Imer, G. O. Ince, T. U. Demir, Y. Z. Menceloglu, S. Unal and I. Koyuncu, *Desalination*, **429**, 20 (2018).
106. P. Pasbakhsh, G. J. Churchman and J. L. Keeling, *Appl. Clay Sci.*, **74**, 47 (2013).
107. M. Naderi, *Prog. Filtr. Sep.*, **585**, 300014 (2015).
108. P. Sinha, A. Datar, C. Jeong, X. Deng, Y. G. Chung and L. C. Lin, *J. Phys. Chem. C*, **123**, 20195 (2019).
109. S. Brunauer, P. H. Emmett and E. Teller, *J. Am. Chem. Soc.*, **60**, 309 (1938).
110. N. Narayanaswamy and C. A. Ward, *J. Phys. Chem. C*, **125**, 28115 (2021).
111. A. K. Panda, B. G. Mishra, D. K. Mishra and R. K. Singh, *Colloid Surf. A Physicochem. Eng. Asp.*, **363**, 98 (2010).
112. P. Yuan, D. Tan and F. Annabi-bergaya, *Appl. Clay Sci.*, **112-113**, 75 (2015).
113. A. Alhuthali and I. M. Low, *J. Mater. Sci.*, **48**, 4260 (2013).
114. U. A. Handge, K. Hedicke-Höchstötter and V. Altstädt, *Polymer*, **51**, 2690 (2010).
115. Z. Shu, Y. Chen, J. Zhou, T. Li, D. Yu and Y. Wang, *Appl. Clay Sci.*, **112-113**, 17 (2015).
116. A. B. Zhang, L. Pan, H. Y. Zhang, S. T. Liu, Y. Ye, M. S. Xia and X. G. Chen, *Colloid Surf. A Physicochem. Eng. Asp.*, **396**, 182 (2012).
117. Q. Wang, J. Zhang and A. Wang, *Appl. Surf. Sci.*, **287**, 54 (2013).
118. Z. U. Zango, N. H. H. Abu Bakar, W. L. Tan and M. A. Bakar, *J. Disp. Sci. Technol.*, **39**, 148 (2017).
119. X. Zeng, Z. Sun, H. Wang, Q. Wang and Y. Yang, *Compos. Sci. Technol.*, **122**, 149 (2016).
120. H. A. Kadir, N. H. H. A. Bakar, N. A. Sabri, F. H. Abdullah, M. A. Bakar and H. Furuno, *Appl. Surf. Sci.*, **531**, 147417 (2020).
121. W. Liu, M. Fizir, F. Hu, A. Li, X. Hui, J. Zha and H. He, *J. Chromatogr. A*, **1551**, 10 (2018).
122. K. Buruga, J. T. Kalathi, K. Kim, Y. Sik and B. Danil, *J. Ind. Eng. Chem.*, **61**, 169 (2018).
123. X. Chen, Y. He, Y. Fan, G. Zeng and L. Zhang, *Sep. Purif. Technol.*, **212**, 326 (2019).
124. A. Kausar, M. Iqbal, A. Javed, K. Aftab, Z. Nazli, H. Nawaz and S. Nouren, *J. Mol. Liq.*, **256**, 3959 (2018).
125. S. S. Imam, A. I. Muhammad, H. F. Babamale and Z. U. Zango, *J. Environ. Treat. Tech.*, **9**, 318 (2021).
126. M. Zhao and P. Liu, *Micro. Meso. Mater.*, **112**, 419 (2018).
127. Y. Xie, D. Qian, D. Wu and X. Ma, *Chem. Eng. J.*, **168**, 959 (2011).
128. A. A. Krasilin, D. P. Danilovich, E. B. Yudina, S. Bruyere, J. Ghanbaja and V. K. Ivanov, *Appl. Clay Sci.*, **173**, 1 (2019).
129. Q. Peng, M. Liu, J. Zheng and C. Zhou, *Micro. Meso. Mater.*, **201**, 190 (2015).
130. M. H. Kanani-jazi and S. Akbari, *J. Environ. Chem. Eng.*, **9**, 105214 (2021).
131. R. S. Hebbar, A. M. Isloor, M. Sohaimi, A. F. Ismail and A. M. Asiri, *J. Taiwan Inst. Chem. Eng.*, **93**, 42 (2018).
132. G. Kiani, *Appl. Clay Sci.*, **90**, 159 (2014).
133. E. Nyankson and R. V. Kumar, *Mater. Today Adv.*, **4**, 100025 (2019).
134. Y. Wang, J. Zhu, G. Dong, Y. Zhang, N. Guo and J. Liu, *Sep. Purif. Technol.*, **150**, 243 (2015).
135. R. Liu, B. Zhang, D. Mei, H. Zhang and J. Liu, *Desalination*, **268**, 111 (2011).
136. P. Luo, Y. Zhao, B. Zhang, J. Liu, Y. Yang and J. Liu, *Water Resour.*, **44**, 1489 (2010).
137. E. Nyankson, B. Agyei-tuffour, E. Annan, A. Yaya, B. Mensah, B. Onwona-agyeman, R. Amedalor and B. Kwaku-frimpong, *Heliyon*, **5**, e01969 (2019).
138. L. Zhu, H. Wang, J. Bai, J. Liu and Y. Zhang, *Desalination*, **420**, 145 (2017).
139. M. Farrokhi-rad, M. Mohammadalipour and T. Shahrabi, *J. Eur. Ceram. Soc.*, **38**, 3650 (2018).
140. J. Ma, Y. He, X. Tang, H. Yu, Y. Fan, T. He and S. Wang, *Sep. Purif. Technol.*, **266**, 118067 (2021).
141. G. Zeng, Z. Ye, Y. He, X. Yang, J. Ma, H. Shi and Z. Feng, *Chem. Eng. J.*, **323**, 572 (2017).
142. G. Zeng, Y. He, Y. Zhan, L. Zhang and Y. Pan, *J. Hazard. Mater.*, **317**, 60 (2016).
143. X. Wan, Y. Zhan, Z. Long, G. Zeng and Y. He, *Chem. Eng. J.*, **330**, 491 (2017).
144. T. Selkälä, T. Suopajärvi, J. Antti, T. Luukkonen, P. Kinnunen, K. I. Kling, J. B. Wagner and H. Liimatainen, *Chem. Eng. J.*, **374**, 1013 (2019).
145. C. Adaobi, S. N. Oba, C. O. Aniagor, A. George and J. O. Ighalo, *J. Ind. Eng. Chem.*, **93**, 57 (2021).
146. S. Elakkiya and G. Arthanareeswaran, *Environ. Resour.*, **204**, 112408 (2022).
147. Z. N. Garba, W. Zhou, I. Lawan, W. Xiao, M. Zhang, L. Wang, L. Chen and Z. Yuan, *J. Environ. Manage.*, **241**, 59 (2019).
148. J. Michałowicz, A. Włuka, M. Cyrkler, A. Maćczak, P. Sicińska and K. Mokra, *Environ. Toxicol. Pharmacol.*, **61**, 95 (2018).
149. B. Szczepanik, M. S. Piotr, D. Bana, A. Kubala-kuku and I. Stabrawa, *Appl. Clay Sci.*, **149**, 118 (2017).
150. R. Natarajan, K. Saikia, S. Kumar, A. Karanam, D. Sri, S. Venkataraman, D. Bharat, V. Arvind, T. Somanna, K. Banerjee, N. Mohideen and V. Kumar, *Chemosphere*, **287**, 131958 (2022).
151. S. Ramanayaka, B. Sarkar, A. T. Cooray and Y. Sik, *J. Hazard. Mater.*, **384**, 121301 (2020).
152. P. Yuan, D. Tan, F. Annabi-Bergaya, W. Yan, M. Fan, D. Liu and H. He, *Clay Clay Miner.*, **58**, 561 (2012).
153. B. Szczepanik, S. Piotr, M. Garnuszek and K. Czech, *Appl. Clay Sci.*, **101**, 260 (2014).
154. F. Salaa, S. Bendenia, G. L. Lecomte-nana and A. Khelifa, *Chem. Eng. J.*, **396**, 125226 (2020).
155. W. A. F. W. AbdulKadir, A. L. Ahmad and B. S. Ooi, *Chem. Eng.*

J., **442**, 129644 (2021).
156. W. Zhang, L. Wang, Y. Su, Z. Liu and C. Du, *Appl. Surf. Sci.*, **566**, 150708 (2021).
157. P. Higgins, S. H. Siddiqui and R. Kumar, *Environ. Nanotechnol. Monit. Manag.*, **17**, 100628 (2022).
158. J. Kurczewska, M. Cegłowski and G. Schroeder, *Appl. Clay Sci.*, **190**, 105603 (2020).
159. M. S. Piotr, B. Szczepanik and M. Garnuszek, *Appl. Clay Sci.*, **114**, 221 (2015).
160. M. T. Viseras, C. Aguzzi, P. Cerezo, C. Viseras and C. Valenzuela, *Micro. Meso. Mater.*, **108**, 112 (2008).
161. R. Zhang, Z. Zhou, A. Xie, J. Dai, J. Cui, J. Lang, M. Wei, X. Dai, C. Li and Y. Yan, *J. Taiwan Inst. Chem. Eng.*, **80**, 424 (2017).
162. R. Zhai, B. Zhang, Y. Wan, C. Li, J. Wang and J. Liu, *Chem. Eng. J.*, **214**, 304 (2013).
163. Z. U. Zango, Z. N. Garba, N. H. H. Abu Bakar, W. L. Tan and M. Abu Bakar, *Appl. Clay Sci.*, **132-133**, 68 (2016).
164. A. Xie, J. Dai, X. Chen, P. Ma, J. He, C. Li, Z. Zhou and Y. Yan, *Chem. Eng. J.*, **304**, 609 (2016).
165. W. Duan, N. Wang, W. Xiao, Y. Zhao and Y. Zheng, *J. Mol. Liq.*, **269**, 874 (2018).
166. R. Janani, B. Gurunathan, K. Sivakumar, S. Varjani, H. Hao and E. Gnansounou, *Environ. Res.*, **203**, 111815 (2022).
167. S. S. Kolluru, S. Agarwal, S. Sireesha, I. Sreedhar and S. Ramdas, *Process Saf. Environ. Prot.*, **150**, 323 (2021).
168. O. O. Okoyomon, H. A. Kadir, Z. U. Zango, U. Saidu and S. A. Nura, *Open J. Environ. Resour.*, **2**, 58 (2021).
169. T. Zhang, W. Wang, Y. Zhao, H. Bai, T. Wen and S. Kang, *Chem. Eng. J.*, **420**, 127574 (2021).
170. A. Aditya, J. Wei, P. Pasbakhsh, F. Hart and A. Talei, *Appl. Clay Sci.*, **160**, 106 (2018).
171. D. Afzali and M. Fayazi, *J. Taiwan Inst. Chem. Eng.*, **63**, 421 (2016).
172. A. Kanti, B. Biswas, R. Naidu and M. Mahmudur, *J. Hazard. Mater.*, **421**, 126812 (2022).
173. R. Hmtshirazi, T. Mohammadi and A. Atabak, *Appl. Clay Sci.*, **220**, 106460 (2022).
174. Z. Fallahnejad, G. Bakeri and A. F. Ismail, *Process Saf. Environ. Prot.*, **157**, 334 (2022).
175. G. Pandey, M. Tharmavaram and D. Rawtani, *Green Energy Technol.*, 125 (2020).
176. Y. Song, P. Yuan, P. Du, L. Deng, Y. Wei, D. Liu, X. Zhong and J. Zhou, *Appl. Clay Sci.*, **186**, 105450 (2020).
177. K. Shehzad, M. Ahmad, C. Xie, D. Zhan, W. Wang, Z. Li, W. Xu and J. Liu, *J. Hazard. Mater.*, **373**, 75 (2019).
178. S. Ahamed, A. Hussam and A. K. M. Munir, *Handbook of Water Purity and Quality*, 379 (2009).
179. W. Jinhua, Z. Xiang, Z. Bing, Z. Yafei, Z. Rui, L. Jindun and C. Rongfeng, *Desalination*, **259**, 22 (2010).
180. N. Ballav, H. J. Choi, S. B. Mishra and A. Maity, *Appl. Clay Sci.*, **102**, 60 (2014).
181. Y. Liu, W. Tu, M. Chen, L. Ma, B. Yang, Q. Liang and Y. Chen, *Chem. Eng. J.*, **336**, 263 (2018).
182. Z. U. Zango, N. S. Sambudi, K. Jumbri, N. H. H. Abu Bakar, N. A. F. Abdullah, E. S. M. Negim and B. Saad, *Chem. Eng. Sci.*, **220**, 115608 (2020).
183. A. Moslehyani, M. Mobaraki, T. Matsuura, A. F. Ismail, M. H. D. Othman and M. N. K. Chowdhury, *Desalination*, **391**, 98 (2016).
184. L. Li, F. Wang, Y. Lv, J. Liu, D. Zhang and Z. Shao, *Appl. Clay Sci.*, **161**, 225 (2018).
185. N. Ballav, H. J. Choi, S. B. Mishra and A. Maity, *Appl. Clay Sci.*, **102**, 60 (2014).
186. W. Jinhua, Z. Xiang, Z. Bing, Z. Yafei, Z. Rui, L. Jindun and C. Rongfeng, *Desalination*, **259**, 22 (2010).
187. Z. Su, H. Zhang, Y. Gao, L. Huo, Y. Wu and X. Ba, *Chem. Eng. J.*, **393**, 124695 (2020).
188. S. Cataldo, G. Lazzara, M. Massaro, N. Muratore, A. Pettignano and S. Riela, *Appl. Clay Sci.*, **156**, 87 (2018).
189. S. Wang, D. Xiao, X. Zheng, L. Zheng and Y. Yang, *J. Environ. Chem. Eng.*, **9**, 106865 (2021).
190. J. Matusik and W. Anna, *Appl. Clay Sci.*, **100**, 50 (2014).
191. Q. Jing, L. Chai, X. Huang, C. Tang, H. Guo and W. Wang, *Trans. Nonferrous Met. Soc. China*, **27**, 16 (2017).
192. M. H. Kanani-jazi, S. Akbari and M. H. Kish, *Adv. Powder Technol.*, **31**, 4018 (2020).
193. S. Mellouk, A. Belhakem, K. Marouf-khelifa, J. Schott and A. Khelifa, *J. Colloid Interface Sci.*, **360**, 716 (2011).
194. C. Shu, C. Chiew, H. Koon, P. Pasbakhsh, K. Krishnaiah, P. Eong, T. Tey and E. Seng, *Appl. Clay Sci.*, **119**, 301 (2016).
195. C. V. Lazaratou, D. Panagiotaras, G. Panagopoulos, M. Pospíšil and D. Papoulis, *Environ. Technol. Innov.*, **19**, 100961 (2020).
196. J. Zare, F. Moeinpour, A. Mirhoseini, S. Ali and Y. Ardakani, *J. Mol. Liq.*, **300**, 112345 (2020).
197. D. Janacek, L. Kvitek, M. Karlikova, K. Pospiskova and I. Safarik, *Appl. Clay Sci.*, **162**, 10 (2018).
198. C. Keong, X. Ying, T. Lim, G. Cheng, B. Amini and B. Salamatinia, *Carbohydr. Polym.*, **138**, 16 (2016).
199. X. Song, L. Zhou, Y. Zhang, P. Chen and Z. Yang, *J. Clean. Prod.*, **224**, 573 (2019).
200. J. Xiao, S. Xie, Y. Jing, Y. Yao, X. Wang and Y. Jia, *J. Mol. Liq.*, **220**, 304 (2016).
201. J. M. Redondo and A. K. Platonov, *Environ. Res. Lett.*, **4**, 014008 (2009).
202. Ihsanullah, H. A. Asmaly, T. A. Saleh, T. Laoui, V. K. Gupta and M. A. Atieh, *J. Mol. Liq.*, **206**, 176 (2015).
203. H. A. Isiyaka, K. Jumbri, N. S. Sambudi, Z. U. Zango, N. A. F. Abdullah and B. Saad, *Int. J. Environ. Sci. Technol.*, **20**, 277 (2023).
204. S. N. W. Ikhsan, N. Yusof, F. Aziz, N. Misdan, A. F. Ismail, W.-J. Lau, J. Jaafar, W. N. W. Salleh and N. H. H. Hairom, *Sep. Purif. Technol.*, **199**, 161 (2018).
205. S. Nazirah, W. Ikhsan, N. Yusof, F. Aziz and A. Fauzi, *Mater. Today Proc.*, **46**, 1978 (2021).
206. G. Zeng, Y. He, Y. Zhan, L. Zhang, H. Shi and Z. Yu, *Ind. Eng. Chem. Res.*, **55**, 1760 (2016).
207. Q. Wang, J. Cui, S. Liu, J. Gao, J. Lang and C. Li, *J. Mater. Sci.*, **54**, 8332 (2019).